NPL REPORT CBTLM 30

Design of a co-ordinate measuring probing system for characterising three-dimensional micro-structures

Richard K Leach, Jennifer Murphy & Alan Wilson

February 2004

Design of a co-ordinate measuring probing system for characterising three-dimensional micro-structures

Richard K Leach, Jennifer Murphy & Alan Wilson
Centre for Basic, Thermal and Length Metrology

ABSTRACT
This report describes research towards a prototype probing system that can be used to determine the geometrical co-ordinates of points on the surface of a three-dimensional micro-structure. Most commercial instruments designed to measure dimensions of micrometre-sized features are essentially planar measuring instruments – they usually have limited range in at least one axis and were originally designed with surface topography measurement in mind. Recent comparisons of commercial systems that measure surface topography give large spreads in the measurement results and it is asserted that this is due primarily to a lack of suitable traceability of the measurements. The report includes a literature review of the current methods for measuring micro-scale components and/or surface topography and this information was used to make a decision on the type of probe that was developed and reported here. The probe described here is capable of measuring three-dimensional features of high aspect ratio, for example, deep trenches, sidewalls and nozzles. The probe is constructed using micro-machining techniques that are described in this report. It is expected that the probe will eventually form the basis for a co-ordinate measuring machine that will be capable of calibrating transfer artefacts that can in-turn be used to calibrate the more versatile commercial measuring instruments.

ISSN 1469-4921

National Physical Laboratory
Queens Road, Teddington, Middlesex, TW11 0LW

Approved on behalf of the Managing Director, NPL
by Dr David Robinson, Head, Centre for Basic, Thermal & Length Metrology

TABLE OF CONTENTS

1 INTRODUCTION 1
2 LITERATURE REVIEW 3
2.1 TACTILE MEASUREMENT SYSTEMS 3
2.1.1 Introduction to contacting probing systems 3
2.1.2 Tactile measurement systems with reduced probing force 5
2.1.3 Summary of tactile measurement systems 6
2.2 SURFACE PROFILE MEASUREMENT SYSTEMS 7
2.2.1 Optical measuring systems 7
2.2.2 Contacting stylus devices 9
2.2.3 Electron microscopy 9
2.2.4 Scanning probe microscopy 10
2.2.5 Summary of surface profile measurement systems 12
3 DESIGN CONSIDERATIONS FOR A TACTILE MICRO-CMM PROBE 13
3.1 MAIN ISSUES 13
3.2 A SIMPLE FLEXURE ARRANGEMENT 15
4 DESIGN OF A PROTOTYPE MICRO-CMM PROBE 17
4.1 NOMENCLATURE 17
4.2 DESIGN OF THE STYLUS TIP 17
4.3 DESIGN OF THE SHAFT 19
4.4 FINITE ELEMENT ANALYSIS 22
4.4.1 Setting up the simulation 22
4.4.2 Calculation of the stiffness of the probing system 25
4.5 ASSEMBLY 28
4.6 OPTICAL DETECTION SYSTEM 28
4.7 ELECTRONIC DETECTION CIRCUITS 30
4.8 SOFTWARE CONTROL AND TRANSLATION STAGE 30
5 EXPERIMENTAL RESULTS 31
5.1 REPEATABILITY TESTS 31
5.2 MEASUREMENTS OF SMALL HOLES 31
6 FUTURE RECOMMENDATIONS 34
7 ACKNOWLEDGMENTS 35
8 REFERENCES 35

LIST OF FIGURES

Figure 1 - Photograph of the NPL Small CMM 4
Figure 2 - Diagram of a flexure arrangement suitable for a nano-probing system.....16
Figure 3 - Probe structure. 17
Figure 4 - Flexure structure. 17
Figure 5 - Elastic compression of a ball on a plane. 18
Figure 6 - Error caused by compression. 19
Figure 7 - Probe with cylindrical stylus tip.....19
Figure 8 - Example dimensions of cylinder.....19
Figure 9 - Beam deflection. 20
Figure 10 - Graph of deflection against force for the tungsten probe.....21
Figure 11 - Bent leg flexure structure. 22
Figure 12 - Straight leg flexure structure. 22
Figure 13 - Solid membrane flexure structure. 22
Figure 14 - Dimensions for each case. 23
Figure 15 - Finite element screenshot of overhead view of finite element model.....24
Figure 16 - Finite element screenshot of side view of finite element model. 24
Figure 17 - Displacement in *z* direction. 25
Figure 18 - Displacement in *x* direction.....25
Figure 19 - Displacement in *y* direction.....25
Figure 20 - Displacement in *xy* direction. 25
Figure 21 - Layout of the optical detection system. 29
Figure 22 - Photograph of the optical layout. 29
Figure 23 - Physik Instrument three axes micro translation stages. 30
Figure 24 - Metal hub. 31
Figure 25 - Results from measurements of a metal hub. 32
Figure 26 - Results from measurements of a ceramic tube.....33

LIST OF TABLES

Table 1 - Design specification for 3D measurement system capable of measuring microstructures....2
Table 2 - Relative characteristics of CMM measurement systems....5
Table 3 - Material properties used for FE models. 18
Table 4 - Displacement of a cylindrical beam. 20
Table 5 - Allowable applied force for elastic deflection. 22
Table 6 - Dimensions for variables....23
Table 7 - Probe stiffnesses. 26
Table 8 - Flexure structure stiffnesses. 27
Table 9 - Maximum contact force for a 2 μm stylus tip displacement 28

1 INTRODUCTION

The rapid development of the microelectronics industry has led to corresponding advances in microsystems technology. Silicon is an extremely good mechanical material that can be micromachined to realise micromechanical structures within the bulk of a single-crystal silicon wafer. These microstructures may cover the thickness range from micrometres to the thickness of the full wafer (200 μm to 500 μm) and the lateral ranges from micrometres to the diameter of the full wafer (75 mm to 200 mm) [1]. The three dimensional features making up these microstructures are extremely small, with potentially high aspect ratios. The ultimate goal of microsystems technology (MST) is the production of micro-electromechanical systems (MEMS) - monolithic or integrated chips that not only sense (with microsensors) but also actuate (with microactuators) [2]. Further advances in the area of MST include the use of non-silicon materials (for example, glasses, polymers and metals) and totally novel machining techniques (for example, deep reactive ion etching, LIGA and laser ablation) that can produce very complex, high aspect ratio structures.

The performance of MEMS type devices will be critically dependent upon the accuracy and integrity with which the devices can be manufactured. The assessment of this accuracy will, therefore, be a key issue in determining whether these new microsystems can achieve the desired functional performance. The requirement to accurately measure the dimensions of micro- and nanometric size features on MEMS devices has led to the development of new types of high precision, high accuracy 3D coordinate measurement machines (CMMs), sometimes classified as micro-or nano-CMMs [3, 4, 5].

Conventional CMMs generally use touch-trigger probes that detect contact between a stylus tip and the surface of the artefact under test. Touching the part physically assures reliable and repeatable measurements. Most touch-trigger probes use a strain gauge or kinematic-resistive type of sensing system that requires a probing force of around 0.1 N or more to activate the switch that triggers the measurement. However, dynamic forces acting at the moment of contact can be much larger than this, around 5 N or more, and can lead to damage of the probed surface. In addition, the smallest stylus tips commercially available have a diameter of around 0.3 mm (for example, the Renishaw A-5000-7800 stylus), placing a lower limit on the dimension of the structures that can be measured using this type of instrument.

Accurate 3D coordinate measurement of MEMS type features will, therefore, require the development of a new family of 3D micro-probing systems. The performance characteristics of these devices will be extremely demanding, combining aspects such as small size, and positioning with extremely high accuracy and low probing force. In addition, it is also desirable that measurements are traceable to National Standards [6, 7].

It is useful at this stage to define the typical shapes and dimensions of the types of microstructures that may require measurement. The features will be truly three dimensional, having length, width and height. The lateral dimensions of the structures may be as small as 10 μm with a range of possible geometries (e.g. walled channels, internal and external cylinders, membranes and cantilevers [8]). The features may have high aspect ratios, with heights (or depths) of as much as 100 μm or more. Ideally a probing system would be able to cope with this demanding range of measurement tasks.

A 'working' specification for a 3D probing system suitable for measurement of microstructures is given in Table 1. A desirable design constraint is that the probing forces are equal in all three axes (this ensures that effects such as probe over-travel and tip deformation are equal in all axes). The values quoted for the performance specification are for indication only rather than a rigid set of design criteria.

Design characteristic	Specification
System characteristics	• 3D measurement system
	• traceable to National Standards
	• working volume 10 mm x 10 mm
	• resolution < 50 nm
	• measurement uncertainty < 50 nm
Probing system characteristics	• stylus tip diameter 10 μm
	• stylus tip form 5 nm
	• stylus shaft length 100 μm
	• probing force < 0.1 mN

Table 1 - Design specification for 3D measurement system capable of measuring microstructures.

Two approaches lend themselves to accurate measurement of 3D form:

- tactile measurement systems, where the test surface is mechanically contacted by some form of probe;

- and non-contacting measurement systems.

The technology relating to both techniques is relatively mature and a brief description of the metrology behind both techniques is discussed below, including comments on their inherent advantages and limitations. A review of the current technology in each field is also included.

Following the literature review, the remainder of this report describes the research and development of a prototype probe that could be used as part of a micro-CMM with the performance characteristics given in Table 1. The design of the probe is presented along with its method of manufacture and finally results that were obtained using the prototype probe mounted on a three-axis movement stage that acted as the CMM metrology for these investigations.

2 LITERATURE REVIEW

2.1 TACTILE MEASUREMENT SYSTEMS

2.1.1 Introduction to contacting probing systems

Tactile (touch) measurement systems are generally some form of co-ordinate measuring machine (CMM). CMMs have three or more measurement axes, usually linear or rotary or a combination of the two. The measurement axes are arranged so that a unique combination of axes positions defines a single point in space. Measuring an object using a CMM is achieved by moving a measuring probe to a number of points on the object surface in sequence and measuring the position of the probe at each point *via* the machine scales. The measurements are then corrected for the diameter of the stylus tip and the direction of contact with the surface (tip correction vector).

A conventional CMM contact probe consists of a ball-ended stylus attached to the probe. A ball shaped tip is used to ensure single point contact with the test artefact. Because the probe tip is located at the end of a long shaft it is remote from the probe sensors that detect contact with the surface under test. This offset, combined with any inevitable tilting of the probe stem, results in an Abbe error. This error is proportional to the sine of the tilt angle and is, therefore, significant even for small tilts.

For common meso-scale engineering parts commercial CMMs with highly accurate geometry and probing heads can fulfil most challenging demands (typical CMM accuracies are around 2-5 parts in 10^6). Improved measurement accuracy can be achieved by scaling down the dimensions of the CMM, reducing *x*-*y* travel and guide length thereby reducing inertia and tilt errors. In addition, a CMM using a design based upon the Abbe and Bryan [9] principles can further reduce measurement uncertainty. A CMM designed by the Precision Engineering Section of Eindhoven University of Technology has been developed with a standard uncertainty below 0.1 μm in a measuring volume of 1 dm^3 [10].

The extension of CMM metrology to smaller structures is limited, primarily by the probing system. The smallest stylus tip diameters of conventional probing systems range from 0.5 mm to 0.2 mm. Stylus tips this size are extremely difficult to handle. In addition, the high probing forces (typically 0.1 N) resulting from the relatively large mass of conventional measuring systems tend to deform the test artefact elastically or even plastically [11], [12].

A number of designs have been investigated to realise a probing system with high accuracy and low probing force. Pril *et al* have developed a 2D probing system with nanometre resolution [13]. In this system the stylus is suspended elastically from the probe housing by three leaf springs in a ‘Manxman’ style triangular arrangement. In this system the probing forces were reduced to several millinewtons using stylus tips with diameters of around 0.3 mm. By reducing the stiffness of the flexure arrangement Peggs *et al* [5] have developed a similar probing system with probing forces as low as 0.1 mN. The measurement uncertainty of the CMM system using this probe was 50 nm within a measurement volume of 50 mm x 50 mm (see Figure 1). The probing system was designed to have an equal probing force in all directions.

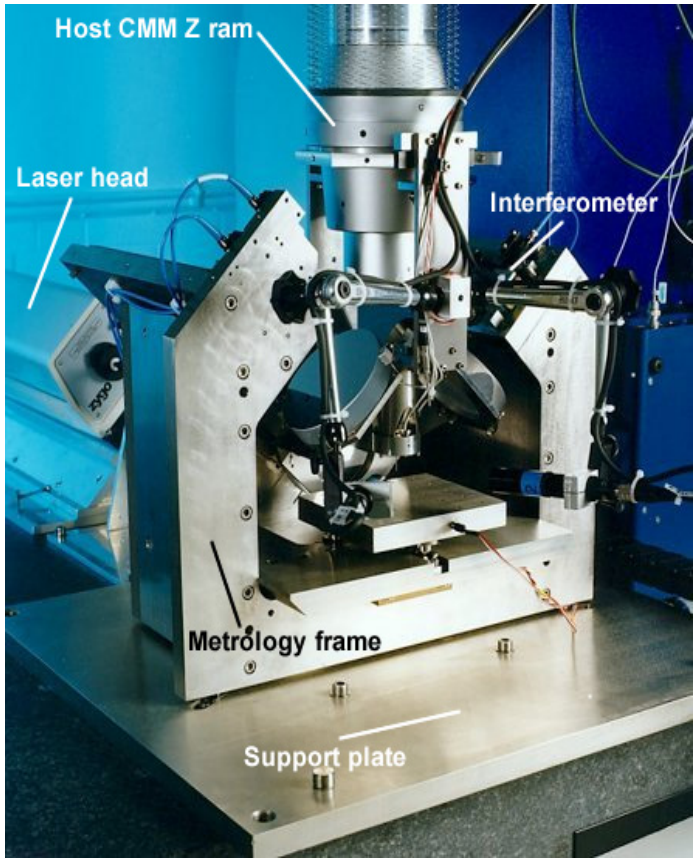

Figure 1 - Photograph of the NPL Small CMM

An alternative to the above approach is to use a silicon membrane in place of the flexures. Haitjema *et al* [14] and Kleine-Besten *et al* [15] have used this approach to attempt to reduce probing forces. In both cases piezoresistive elements were deposited onto the silicon membrane to detect three-dimensional deformation. The diameter of the stylus tip used in both cases was 0.3 mm. The probing forces observed with this design can be further reduced by replacing the full membrane by an arrangement of membrane strips [16]. The probing force achieved by the stripe membrane system was around 100 mN in the horizontal direction. However the probe did not exhibit equal stiffness in all probing directions.

A probing system proposed by Enami *et al* [17] uses an optical technique to detect movement of the stylus tip on contact with a test artefact. A laser beam is focussed and directed through a hollow stylus onto a specularly reflecting stylus ball. A small lens within the stylus is used to bring the beam to a virtual focus at the centre of the ball. The centre of the ball therefore acts as a virtual source of light. The reflected beam from the surface of the ball is focussed onto a quadrant photodetector. When the stylus tip comes in contact with a surface the ball will shift normal to the laser beam. The virtual light source will, therefore, also shift. The photodetector is used to detect the displacement of the laser spot. A resolution of less than 10 nm has been reported for this system. However, the performance of the probing system in the vertical direction is unknown.

A similar probing system using optical detection has been reported by Furutani *et al* [18]. In this system a conventional type probe stylus is rigidly supported from a disc shaped elastic hinge. A ball lens is attached to the stylus at the opposite end to the probe ball. Laser light is directed through the upper part of the stylus and is focussed onto the centre of a quadrant

photodetector by the ball lens. When the probe contacts a surface the spot moves from the centre of the detector. This type of probing system has reduced overtravel thus reducing probing forces. The probing forces of this system in the *x*- and *z*-directions were 0.07 μN and 0.4 μN respectively.

Measurement of structures at the micro- or nanometre level will necessitate the use of probing systems with low probing forces and small stylus tip diameters. In addition, the form error of the stylus tip must be at least an order of magnitude better than the desired uncertainty of measurement of the artefact under test. Table 2 shows a comparison of typical specifications for members of the CMM family indicating the characteristics necessary to realise measurements at the nanometre level.

Characteristic	CMM	Small CMM	Micro-CMM
range	1 m x 1 m	50 mm x 50 mm	10 mm x 10 mm
resolution	1 μm	100 nm	10 nm
probe diameter	1 mm	300 μm	10 μm
probe ball form	1 μm	50 nm	5 nm
probing force	0.1 N	1 mN	< 0.1 mN

Table 2 - Relative characteristics of CMM measurement systems.

2.1.2 Tactile measurement systems with reduced probing force

In order to reduce problems arising from the relatively high static and dynamic probing forces arising from touch-trigger type probes Schwenke *et al* [19] have developed an opto-tactile probing system with greatly reduced probing force. The system uses an optical fibre with a spherical tip as the probing stylus. Launching light into the fibre illuminates the tip of the fibre. Light backscattered from the spherical tip is imaged as a bright spot on a CCD camera mounted vertically above the fibre. When the probe tip contacts a surface the position of the spot on the CCD array is changed. Measurement in 3D is achieved by adding a second illuminated target vertically displaced up the fibre, the position of this target being monitored on a second CCD camera arranged perpendicularly to the fibre. Stylus tip diameters of 25 μm with stylus shaft diameters of 15 μm have been manufactured for use with this system. Probing forces achieved with this system were around the 10 μN level. This type of probe was considered as a candidate for further development, but it has not been found to operate well in 3D.

An alternative technique that can be used to reduce probing forces is through the use of a high frequency resonating stylus (Apollo Research Corp., West Seneca, USA). The probing system attaches to a conventional CMM. The probe body has a crystal oscillator inside of it that creates a vibration in the stylus. The probe stylus resonates at 20 kHz to 25 kHz and a second crystal detects this vibration. When the stylus contacts a surface, the vibrational motion changes and the change is detected by an electronics system, which signifies this change as a probing event. Unlike conventional touch trigger probes, which require several grams of force to trigger, this type of probe will trigger on less than 1 μN force. Matsuoka *et*

al [20] have reported a similar probe system, based upon detecting the change in resonance of a cross-shaped leaf spring. A measurement repeatability of 300 nm with a probing force of less than 50 μN has been reported for this system.

A resonant type probe has been used to measure the profile of small holes [21]. This system uses a pair of adjacent cantilever elements to form the probe with a small voltage applied between the elements. The elements are isolated electrically to stop them coming into contact with each other. The two elements are vibrated in parallel with a small amplitude. When the probe comes into contact with a surface the front element is deflected and comes into contact with the second element. The profiles of holes with diameters as small as 125 μm have been measured using this system, with measurement uncertainties of the order of 0.5 μm. However, it must be noted that this system is not a true 3D system and can only measure profiles in 2D. In addition, the probe tip uses an edge point to contact the test surface.

Although it is true that commercially available resonant type probes have reduced probing forces, the stylus tips used are relatively large (the Apollo CMM probe uses a stylus tip ball with diameter 1 mm). In addition, the sensitivity of the system may not be the same in three directions; the probe will be more sensitive in the direction of vibration than in a direction perpendicular to this. Also, the response of the system is dependent upon the nature of the surface being probed [22].

Two further methods of contact probing deserve mention. Takamasu *et al* [23] have reported a pneumatic ball probe that consists of a small stylus tip located at the end of a hollow stylus shaft. The ball is held by vacuum pressure to the end of the shaft. When the ball touches a surface it is unseated from its position on the end of the stylus. Air flows from the outside to the inside of the tube and this flow is detected by a differential pressure gauge. The pneumatic ball can, therefore, be used as a touch trigger type probing system. The target resolution of this probe is 1 μm, with a target probing force of 1 μN. The disadvantage of this system is that it only measures in 2D.

A second novel probing technique has been proposed by Takaya *et al* [24] and uses a laser-trapped microsphere as a contact probe. The principle of measurement is based on the laser trapping technique, where a small dielectric sphere is levitated against gravity by the affection of radiation pressure [25]. The levitated sphere is arranged such that it acts as a moving mirror in a Mirau interferometer. When the sphere is in contact with a surface the fringe pattern seen at the output of the interferometer changes. The arrangement of this system is complex and its practicality is unknown at this time. However the target resolution of the system is 10 nm with a probing force of 10 nN. In addition, the proposed probe sphere diameter is 10 μm and the ability to produce spheres of this size with an appropriate form figure is of interest

2.1.3 Summary of tactile measurement systems

During the last few years a number of researchers have reported the development of probing systems designed to provide 3D measurements of microstructures. The most successful of these designs, capable of providing truly 3D co-ordinate measurements, have been tactile systems. A number of different probe configurations have been investigated with the best of these quoting a measurement resolution of less than 10 nm.

The main design issue in the development of a micro-/nano-measuring instrument is the need to reduce the probing forces exhibited by the probe system. One promising approach is through the use of a silicon membrane acting as a 3D flexure. However, prior to the work reported here, the optimal geometry of such a membrane has yet to be defined. In addition it was not known if such an arrangement can meet the desired design criteria of equality of probing force in all directions.

The majority of the reported probing designs have used standard CMM probe styli, with stylus tips of diameter 0.3 mm or more. This will obviously be too large to probe the majority of envisaged microstructures, whose dimensions will typically be of the order of a few tens of micrometres. The smallest balls available from precision bearing manufacturers are around 0.2 mm in diameter (Atlas Ball & Bearing Co Ltd supply a grade 10, silicon carbide ball of this diameter). However, these are non-stock items and cannot be manufactured in small quantities, except at extremely high cost. An alternative source of small spheres is the microscopy industry where microspheres are used to calibrate a variety of scanning probe microscopes. These spheres are available with a range of diameters down to as small as 10-μm. The form error of these spheres is, however, unknown.

A further consideration is the choice of transducer mechanism used to detect probe (or more accurately flexure) deflection due to the probing process. Three techniques offer themselves for this mechanism: capacitive sensing, optical sensing and strain gauge sensing. The final choice will be defined by the desired sensitivity of the probing system.

An inspection of the characteristics given in Table 1 shows that the design specification of a micro-CMM will be extremely demanding. Although some of the reported probe designs meet one or two of the target design criteria, none of them meet them in their entirety. Demonstration of a miniature 3D probe system will require that a number of manufacturing and metrological design issues be properly and successfully addressed. Some of these design considerations are discussed in the following section.

2.2 SURFACE PROFILE MEASUREMENT SYSTEMS

A number of techniques can be used to measure the surface roughness of a sample. These techniques cannot be thought of as truly 3D since the range of vertical measurement which can be achieved is limited, the measurements made being more accurately described as topographical. However, for completeness, a brief summary of these techniques is given below.

2.2.1 Optical measuring systems

The simplest form of optical measuring instrument used is the differential focus microscope [26]. Differential focus microscopes utilise the principle of depth discrimination to determine the surface profile of a sample. A convergent laser beam is projected onto the surface under test *via* a focusing lens, with the reflected light being directed onto a point detector. The vertical position of the focusing lens can be varied *via* a piezo-electric actuator, with the movement of the lens controlled by a focus error signal. As the laser is moved over the test object the focusing lens maintains a precise distance from the object surface through a servo system from the detector to the lens translation circuit. The error signal will, therefore, be a representation of the surface roughness. Measurement in 3D is realised by either scanning the test surface beneath the laser using a precision *x*-*y* table or translating the measurement head

in the *x*-*y* plane while the test artefact is held stationary. Other focus detection methods can be used including the critical angle method, the skew beam method and the confocal method [27].

A number of drawbacks arise with such focus detection systems. The resolution of such a system will be diffraction limited, around 150 nm for incident light at λ = 633 nm. Also, focus detection systems require a finite amount of light to be reflected back to the detector and consequently low reflectivity surfaces cannot be measured reliably. Errors in the surface data can arise when steep slopes are encountered because the scanning spot invariably loses focus and servos rapidly in the *z*-plane for a short period before finding the surface once more. Smooth, sloped surfaces can also cause data errors arising from optical interference between light returning from adjacent areas that are out of phase because of the slope. In both cases the data errors manifest themselves as rogue spikes and pits in the surface of the test artefact.

Nanometre surface resolution can be achieved using optical interference techniques. These systems work on the principle of interfering two beams of light, at least one of which is reflected off the surface under test. The systems are mainly based upon the Michelson or Fizeau interferometers and the two most widely used techniques are phase shifting interferometry and scanning differential interferometry.

In phase shifting interferometry [28] a reference surface is built into an interferometer within the microscope. Light reflected from the test surface interferes with light reflected from the reference surface, the resulting interference pattern being recorded on a CCD array. Deviations in the fringe pattern are related to height variations in the test surface. By changing the phase between the interfering wavefronts in a series of controlled steps and processing the interferograms produced using appropriate algorithms, quantitative measurements of the test surface can be obtained. Phase stepping of the reference surface is normally achieved by driving the reference surface using a piezo-electric stage. The Zygo Mark GPI laser interferometer makes use of the phase shifting technique for 3D surface measurement. This system has a vertical resolution of 2 nm, with a vertical range of 0.1 mm. The horizontal resolution of this instrument is 10 μm and the maximum size of surface that can be measured is 150 mm.

The vertical range of a phase shifting interferometric system is limited to a few hundred micrometres. A technique that can extend this range, based upon white light interferometry, is vertical scanning interferometry (for example, the Zygo NewView 5000 [29]). Here the system measures the degree of fringe modulation or coherence of the interferogram produced between the reference and measurement wavefronts. During measurement the interferometer optics are scanned vertically above the test surface using a piezo-electric stage and the *z*-position of the maximum modulation of the interference fringes are detected. The vertical range of such a system is around 5 mm with a vertical resolution of 0.1 nm. The lateral resolution of this system is from 0.68 μm to 11.8 μm dependant upon the objective lens used.

Rapid slope changes can also cause problems for interferometric systems arising either through insufficient returned light or fringe ambiguities caused by phase discontinuities. In addition, interferometric measurement systems require a high degree of environmental and vibrational isolation in order to stabilise the optical path of the measurement and reference beams.

2.2.2 Contacting stylus devices

A contacting stylus measurement system is one that uses a mechanical contact with a solid probe to measure the change in displacement of the stylus tip as it is traversed across the test surface. These systems generally consist of a probe, a device to support the probe while converting its motion into an electrical signal, and a device to analyse the measured data and display the evaluated value. In profile measurement, a trace of the surface profile is obtained by allowing the stylus to scan mechanically over the test surface in one direction to measure the co-ordinates of consecutive points on the surface profile.

The main drawback of mechanical stylus instruments arises through the high forces generated at the stylus contact point. The surface of the artefact under test can be damaged during measurement. In addition, the stylus can become damaged such that the interaction with the test surface is not constant over time.

2.2.3 Electron microscopy

There are two main types of electron microscopy that are used to image MST devices and these are described below.

Transmission electron microscope

The transmission electron microscope (TEM) operates on the same basic principle as a light microscope but uses electrons instead of light. The active components that comprise the TEM are arranged in a column, within a vacuum chamber. An electron gun at the top of the microscope emits electrons that travel down through the vacuum towards the specimen stage. Electromagnetic electron lenses focus the electrons into a narrow beam and direct it onto the test specimen. The majority of the electrons in the beam travel through the specimen. However, depending on the density of the material present, some of the electrons in the beam are scattered and are removed from the beam. At the base of the microscope the unscattered electrons hit a fluorescent viewing screen and produce a shadow image of the test specimen with its different parts displayed in varied darkness according to their density. This image can be viewed directly by the operator or photographed with a camera.

Using suitable electro-magnetic lenses, TEMs can achieve image magnifications of over x300000 and have extremely high resolutions; a typical TEM can have a resolution of better than 0.5 nm (compared to light microscope magnifications of x1000 and resolutions of 0.2 μm). However, a TEM only produces a 2D image of a test specimen. In addition, electrons have very little penetrating power, so the test specimen must be very thin to allow the electrons to pass through.

Scanning electron microscope (SEM)

An image of a test specimen can be obtained using a scanning election microscope (SEM). This microscope uses a very fine beam of electrons, which is made to scan the specimen under test as a raster of parallel contiguous lines. Upon hitting the specimen electrons will be backscattered or emitted (secondary electrons) from the test surface. The specimen is usually a solid object and the number of secondary electrons emitted by the surface will depend upon its topography or nature. These are collected and amplified and analysed before modulating the beam of a cathode ray tube scanned in sympathy with the scanning beam. The image

resembles that seen through an optical lens but at a much higher resolution. Typical SEMs can achieve image magnifications of x200000 and have a resolution of around 5 nm.

A major drawback with the systems described above is that the probing of the test surface must take place in a vacuum. In addition, in the case of SEMs, the surface under test must be conducting.

2.2.4 Scanning probe microscopy

Scanning probe microscopes (SPMs) are a family of instruments that are used to measure properties of surfaces. Instruments that fall into this category include atomic force microscopes (AFMs) and scanning tunnelling microscopes (STMs). The main feature that all SPMs have in common is that the measurements are performed with a very sharp probe operating in the near field, that is, scanning over the surface while maintaining a very close spacing to the surface. These instruments, specifically STMs, were the first to produce real space images of atomic arrangements on flat surfaces. SPMs are now most commonly used to perform high precision, 3D measurements on the nanometre to micrometre scale.

The STM was the first SPM and was invented by G. Binnig and colleagues [30] in 1981 at the IBM laboratories in Zurich. The STM works by mechanically scanning a sharp conducting tip over the surface of a conducting sample. A bias voltage is applied between the tip and the sample that causes a quantum mechanical tunnelling current to flow when the tip is near the sample (~ 1 nm). The tunnel current is exponentially proportional to the tip-sample separation. Therefore, a small change in this separation results in a large change in the tunnel current. As a consequence of this dependency the STM can employ piezo-electric ceramic drives to accurately control the position of the tip above the sample surface and, hence produce images of surface topography.

The resolution of an STM depends on the geometry of the tip and the sample and on their respective electronic structure, however, a typical vertical resolution of 0.05 nm can be achieved over a typical scan range of 90 μm x 90 μm x 6 μm in the *x*-, *y*- and *z*-directions respectively (for example, the Dimension 3100 manufactured by Veeco Instruments).

STMs are widely used in both industrial and fundamental research to obtain atomic-scale images of conducting and semiconducting surfaces. It provides a three-dimensional profile of the surface that is very useful for characterising surface roughness, observing surface defects, and determining the size and conformation of molecules and aggregates on the surface. It is even possible to use the STM as a molecular manipulator to position individual atoms over a surface. The principle drawback of the STM is that both the surface under test and the probe tip must be conductors or semi-conductors. However, this limitation can be overcome by using a different type of SPM, namely the atomic force microscope.

The AFM is similar in design to the stylus profilometer but uses a sharper probe tip and lower probing force to provide better resolution information without test sample damage. The AFM operates by measuring attractive or repulsive forces between a tip and the test sample [31]. The probe tip, having dimensions of several micrometres in length and 10 nm in diameter, is located at the free end of a cantilever. Applied forces between the tip and the test surface cause the cantilever to bend or deflect. Motion of the cantilever is detected using an optical lever, or beam deflection system [32].

The AFM can be operated in two principal modes; *contact mode* and *non-contact mode*. In contact AFM the probe tip is constantly in contact with the sample surface. Surface contours bend the cantilever. The cantilever is adjusted to maintain a pre-determined bending and the adjustment required is monitored as a function of position on the surface. Disadvantages of this method include the attractive effect of adsorbed liquid on the sample surface and electrostatic forces which introduce both compressive and shearing forces as the tip is dragged over the sample surface. These problems can make measurement difficult and can damage the surface of soft samples. A refinement to this approach is classified as *tapping mode*.

In tapping mode the tip does not contact the surface but senses the weak Van der Waals force between the tip and the sample. The cantilever is usually vibrated at small amplitude and experiences a shift in its resonant frequency due to the interactive forces.

Modern AFMs have 5 nm lateral and 0.01 nm vertical resolutions on all types of test surface. In addition, they can measure over lateral working volumes of up to 200 mm^2. However, the vertical range of a typical AFM is only around 5 μm. NPL have modified a commercially available AFM, adding laser interferometers to the measuring axes of the instrument, enhancing the resolution of this instrument in contact mode in all its axes to around 1 nm [33].
A further technique that has developed from the progress made in the STM and AFM methods is scanning near field optical microscopy (SNOM) [34]. SNOM is an imaging technique that combines the high resolution of a scanning probe microscope (SPM) with the contrast capabilities and mechanisms of conventional optical microscopy.

SNOM is high resolution optical microscopy realised by scanning a small spot of 'light' over the specimen and detecting the reflected (or transmitted) light for image formation. In this case the 'probe' is a single-mode drawn optical fibre with a tiny, optically transparent aperture at its tip. The diameter of the aperture is in the range from 50 nm to 100 nm, *i.e.* smaller than half the wavelength of visible light. Light cannot pass through such an aperture; however, an evanescent field protrudes from it. The optical near-field decays exponentially with distance, and is thus only detectable in the immediate vicinity of the tip.

If the aperture is brought in close proximity to a sample surface, the presence of the sample causes a disturbance of the optical near field, which leads to the emission of light from the location opposite to the aperture. Scanning the aperture at a distance of typically about 10 nm from the sample, and simultaneously detecting either emitted light either in reflection or transmission mode produces a high-resolution optical image. In a typical SNOM set up, the probe is held fixed while the sample is scanned employing the same piezoelectric technology found in most commercial scanning probe microscopes.

The resolution of the SNOM image is defined by the size of the aperture (in contrast to conventional optical microscopy which relies on observation in the so-called far-field, with the achievable resolution limited by diffraction). A typical SNOM has a vertical resolution of around 50 nm with a lateral resolution of 100 nm. The scan range of these devices is typically 100 μm x 100 μm x 20 μm in the *x*-, *y*- and *z*-directions respectively (for example, the AlphaSNOM manufactured by Witec). A SNOM can detect changes in the optical properties of a surface such as variation in the optical constants and luminescence as well as the surface topography.

SNOM instruments are technically closely related to AFMs and STMs, since the probing involves scanning of either the probe tip or the sample, together with a tip/sample distance regulation. Because of this the SNOM can be combined with AFM and STM in a single instrument.

All the SPM methods have advantages and disadvantages. For example, although STM delivers atomic resolution images, it requires electrically conducting samples. AFM operates with the probe forced against the sample surface, with the consequence that the surface may be damaged during measurement. In addition, the scanning probe methods generate (usually) topographic images, with simple height or shape images. SNOM works with any sample and is non-contacting but has lower resolution than AFM or STM at present.

The performance of a scanning probe instrument is limited by a number of factors. One of these is the resolution of the mechanical components used to move the tip and measure its position. The sharpness and stability of the probe tip determine the area of contact and the reproducibility of imaging. Obviously, environmental vibrations must be controlled to a high degree. In addition, most positioning stages depend on piezoelectric drives, which are subject to problems of non-linearity and to overshoot during rapid movements [35].

2.2.5 Summary of surface profile measurement systems

A large number of instruments are available for surface topography measurement. Non–contact instruments such as phase-shifting and white light interferometers can achieve nanometre resolution on regular surfaces. Adding a scanning stage to the *z*-axis positioning actuator can enhance the vertical range of white light systems. However, measurement errors can occur when using these systems to measure surfaces with rapid slope changes.

Electron microscopes can also be used to provide topographical surface information. However, the requirement of a conducting or semi-conducting test surface, and the fact that testing must take place in a vacuum column places restrictions on this approach.

Scanning probe microscopy covers several related technologies for imaging and measuring surfaces on a fine scale, down to the level of molecules and groups of atoms. SPM technologies share the concept of scanning an extremely sharp tip across the test surface. Scanning probe microscopes are already being used to study MEMS devices [36] providing high precision metrology of devices and features. A Veeco AFM has been used to measure digital micro-mirror devices produced by Texas Instruments. Among the measurements made on these devices were mirror planarity, mirror surface smoothness and mirror spacing. It is also possible to use an AFM to measure features with steep slopes by using special, high aspect ratio measuring tips.

The principle drawback with all these systems is that they only capable of topographical measurements and cannot provide truly 3D co-ordinate measurements of complex microstructures.

3 DESIGN CONSIDERATIONS FOR A TACTILE MICRO-CMM PROBE

3.1 MAIN ISSUES

The literature review demonstrates that there is no simple, existing technique capable of measuring 3D microstructures. However, an incremental development of the contacting probe described in this section would seem to be promising. The following section describes the key design issues that need to be addressed in order to produce such a probe.

Stylus tip diameter

The dimensions of the features to be probed will determine the diameter of the stylus tip used. It is apparent that very small features will require a very small stylus tip, for example, a channel of width 50 μm will necessitate a stylus tip of diameter around 20 μm or less to allow the dimension of the slot to be measured. However, a reduction in size of the stylus tip to these dimensions will greatly increase the handling and manufacturing difficulties. As noted above, small probe balls of a known quality with diameters below 0.3 mm are not generally available from either CMM or precision bearing manufacturers.

Stylus tip form

The form error of the stylus tip ball must be at least an order of magnitude better than the desired measurement uncertainty of the artefact under test. Although the manufacture of high quality micro-spheres has been reported (SRM 1960 ‘space beads’ 10 μm in diameter), the form error of these artefacts is unknown. If the form error of the stylus tip is not known it must somehow be determined through some qualification process. A method of directly measuring extremely small spheres to the desired accuracy is not known at this time. It may be possible to qualify the probing system by taking a series of measurements of a high quality reference sphere. In this case the resulting measurement errors will be a combination of errors relating to the form of the probe ball and other errors present in the probing system (*i.e.* flexure non-linearities, hysteresis, *etc.*)

Stylus shaft length

The depth of the features that need to be probed will effectively determine the probe shaft length. Ideally, the probe shaft should be as short as possible, thereby making the shaft as stiff as possible. Bending of the probe shaft can occur on contact if longer probe shafts are used due to the reduced stiffness of the shaft.

Stylus shaft stiffness

The stylus shaft should be as stiff as possible to avoid bending of the shaft during probing. Suitable materials are tungsten carbide or stainless steel. Hardened steel drill blanks can be purchased with diameters as small as 150 μm. An alternative choice of material is glass fibre, which can be drawn into extremely small cross sectional dimensions.

The stem should, however, be made from as light a material as possible to minimise the weight of the probing system. This would make a probe shaft made from capillary tube a

potentially ideal choice. However, capillary tube is not readily available in dimensions much less than 0.2 mm outside diameter

Stylus shaft diameter

The diameter of the probe shaft must obviously be less than that of the stylus tip while remaining as stiff as possible. In addition, the stylus tip should be sufficiently small to provide adequate clearance such that the shaft cannot touch the surface of the artefact under test ahead of the contact by the stylus tip. The use of stylus shafts with extremely small diameters once again increases the manufacturing and handling difficulties.

Probing force

The probing force should be such that contact of the stylus tip with the surface under test does not damage the surface. The probing force is in fact a combination of three forces:

(a) The collision force that occurs when the stylus tip first touches the surface of the test artefact. The moving parts of the probe have to be decelerated, leading to forces between the probe and the artefact. During this collision the probe may bounce once or several times.

(b) The overtravel force. After receiving a stop signal from the probe, the moving stage of the CMM travels a further distance called overtravel, which stretches the probe flexures leading to an elastic force between the probe and the test artefact.

(c) Measuring force. The force that occurs between the probe and the test artefact when a data point is recorded. This force is generally much smaller that the collision and overtravel forces.

The magnitude of these forces are dependent upon a combination of parameters including the moving mass of the probe, the Young's moduli and Poisson ratios of the stylus tip and the test surface, the stylus tip radius and the probing speed. In order to minimise these forces the probe should be as light as possible and the surface should be probed as slowly as possible. These criteria obviously place severe limitations on the design of the probing mechanism, the resolution of the probe drive mechanisms and the minimum time taken to probe a test artefact. A further consideration involves the diameter of the stylus tip and the pressure exerted on the test surface as the probe touches. Since the surface pressure is force per unit area the pressure will be minimised by using as large a stylus tip diameter as possible. This requirement is obviously in conflict with point about the stylus tip above.

Probe weight

The mass of the probing system should be as low as possible to minimise the probing forces. The materials used should, therefore, be light and stiff.

X-Y-Z stage resolution

It is necessary that the resolution of the linear motion slideways used to manipulate the probing system around the structure to be measured are of the same order as the desired measurement resolution. In other words if a 3D measurement resolution of 50 nm is desired, the resolution of the motion of the *x*-, *y*- and *z*-slideways should be approximately 25 nm.

Piezoelectric positioning stages are commercially available with resolutions of a few nanometres. However, the positioning system will need to be pre-calibrated, or fitted with an alternative form of metrology, for example, length measuring laser interferometers to ensure the desired positional accuracy due to non-linearities and hysteresis typically seen in piezo-electric actuators.

Environmental considerations

The desired system measurement resolution demands that both the probe and the artefact under test must be kept clean from contamination. Particles of dirt and dust can have dimensions up to a few micrometres, approximately the same dimension as the stylus tip. These particulates are extremely difficult to remove from a surface, especially from the probing system where contact cleaning may damage the probe or flexures. Thermal and mechanical (both seismic and acoustic) effects must also be taken into consideration.

3.2 A SIMPLE FLEXURE ARRANGEMENT

A possible flexure arrangement for the probing system is shown in Figure 2 below (the arrangement is similar to that proposed by Haitjema *et al* [14]). The diagram is not to scale.

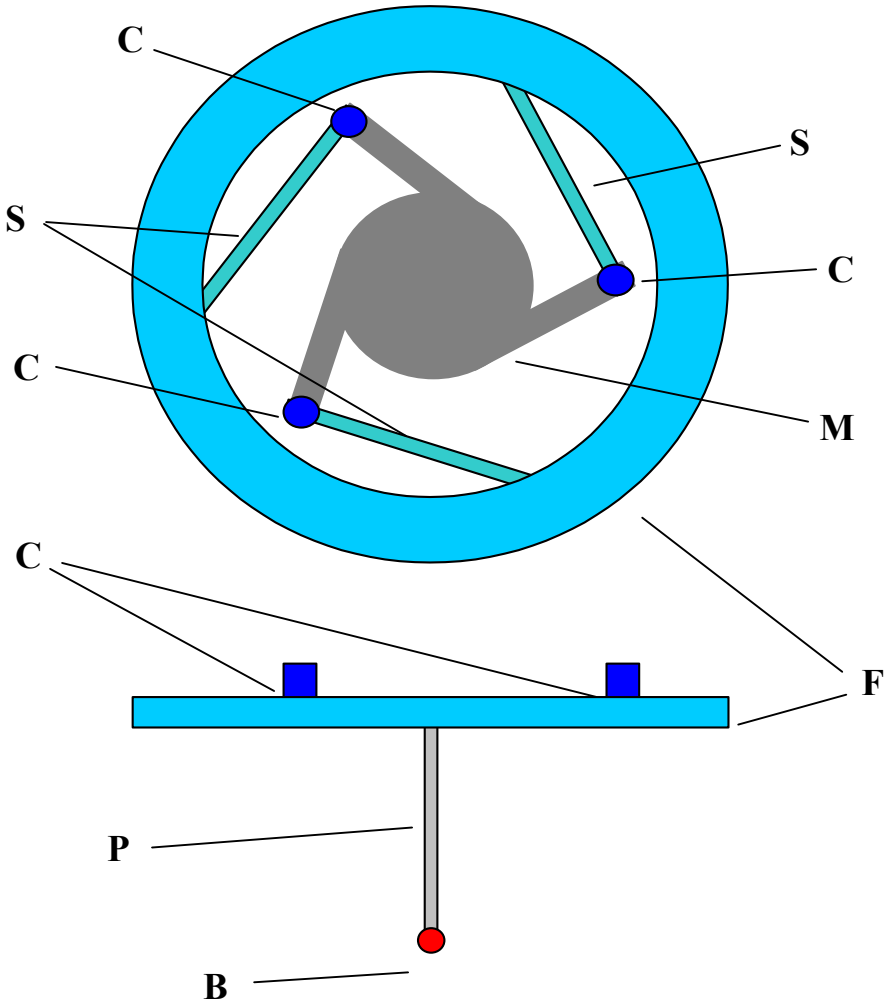

C ; Displacement sensor **S ; Strip flexure**
M ; Silicon membrane **P ; Stylus Shaft**
F ; Support frame **B ; Stylus tip**

Figure 2 - Diagram of a flexure arrangement suitable for a nano-probing system.

4 DESIGN OF A PROTOTYPE MICRO-CMM PROBE

4.1 NOMENCLATURE

Figure 3 and Figure 4 show the nomenclature that will be used throughout the rest of this report. The probe refers to the upper shaft, lower shaft and stylus tip. The flexure structure refers to the central island and the legs. The probing system refers to the combination of the probe and the flexure structure.

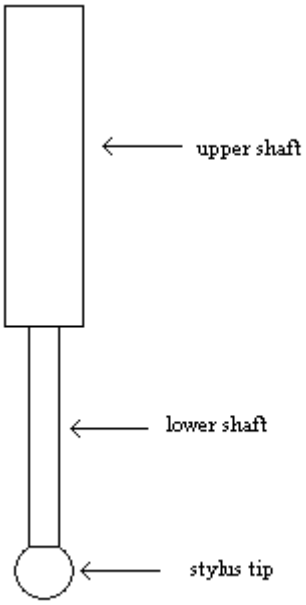

Figure 3 - Probe structure.

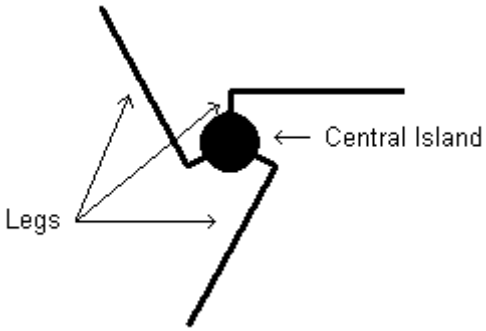

Figure 4 - Flexure structure.

4.2 DESIGN OF THE STYLUS TIP

For the stylus tip, it was important to use a sphere small enough to enter into small holes, but large enough to reduce the amount of elastic compression between the surface and the sphere (see Figure 5). To calculate the amount of elastic compression between the sphere and the probing surface, the equations due to Hertz were used. These equations assume that the surfaces in contact are perfectly smooth, that the elastic limits of the materials are not exceeded, that the materials are homogeneous and that there are no frictional forces within the contact area. These assumptions may not always apply for very small stylus tips.

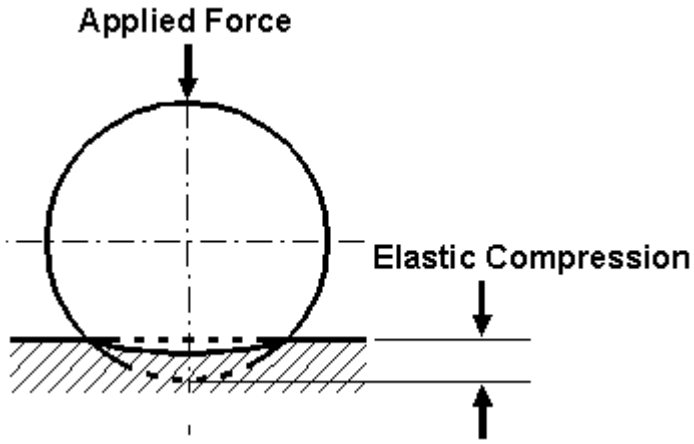

Figure 5 - Elastic compression of a ball on a plane.

The amount of elastic compression for a sphere on a planar surface is given by

$$\alpha = \frac{(3\pi)^{\frac{2}{3}}}{2} P^{\frac{2}{3}} (V_1 + V_2)^{\frac{2}{3}} \left(\frac{1}{D}\right)^{\frac{1}{3}}, \tag{1}$$

with

$$V_1 = \frac{(1-\sigma_1^2)}{\pi E_1} \tag{2}$$

and

$$V_2 = \frac{(1-\sigma_2^2)}{\pi E_2} \tag{3}$$

where P is the applied force, D is the diameter of the sphere, σ_1 and σ_2 are the Poisson's ratios and E_1 and E_2 are the Young's modulae of the stylus tip and surface materials respectively [37]. The material properties used for the calculations can be found below in Table 3.

Material	**Young's modulus, E (N m^{-2})**	**Poisson's ratio, σ**	**Density, ρ (kg m^{-3})**
Nickel	2.07 x 10^{11}	0.30	8.9 x 10^{3}
Tungsten	4.00 x 10^{11}	0.28	19.3 x 10^{3}

Table 3 - Material properties used for FE models [38].

It is important to minimise the elastic compression, because a large elastic compression can result in either the sphere or the planar surface compressing and causing the probe to give a false or unpredictable measurement. A large compression will cause an error in surface measurements because the surface will appear to be further away from the base of the probe than it actually is (see Figure 6).

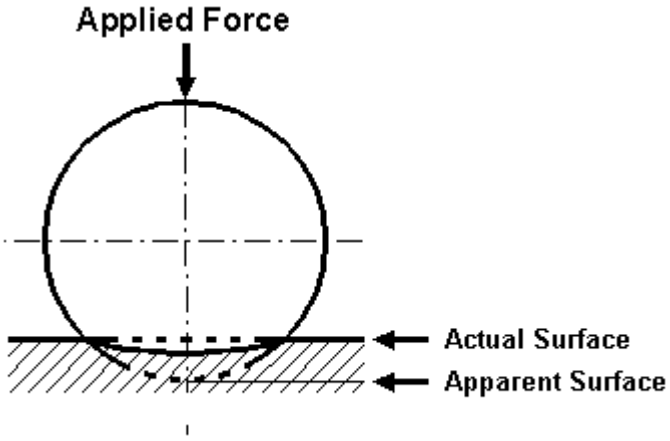

Figure 6 - Error caused by compression.

The planar surface materials used for the Hertzian compression calculations were steel, silicon, aluminium and polystyrene. The stylus tips for these experiments (manufactured at the National Taipei University of Technology, Taiwan) were made of tungsten and had a diameter of nominally 50 µm. For an applied force of 1 mN, the elastic compression of tungsten on steel, silicon and aluminium is between 10 nm and 20 nm, which is within an acceptable limit for this prototype design. The elastic compression for a tungsten sphere on a polystyrene planar surface was much larger than 20 nm, so polystyrene would not be a good surface for a tungsten probe because of the large error in measuring the location of the surface.

4.3 DESIGN OF THE SHAFT

Two types of probes were used for these experiments. The University of Tokyo, Japan [39] manufactured several probes with cylindrical stylus tips with a diameter of 50 µm, an upper shaft diameter of 350 µm, a lower shaft diameter of 30 µm and lower shaft lengths of 500 µm, 1000 µm, 1500 µm and 2000 µm (see Figure 7 and Figure 8). The National Taipei University of Technology, Taiwan manufactured several styli with spherical stylus tips with a diameter of 50 µm, an upper shaft diameter of 350 µm, a lower shaft diameter of 30 µm and a lower shaft length of 500 µm.

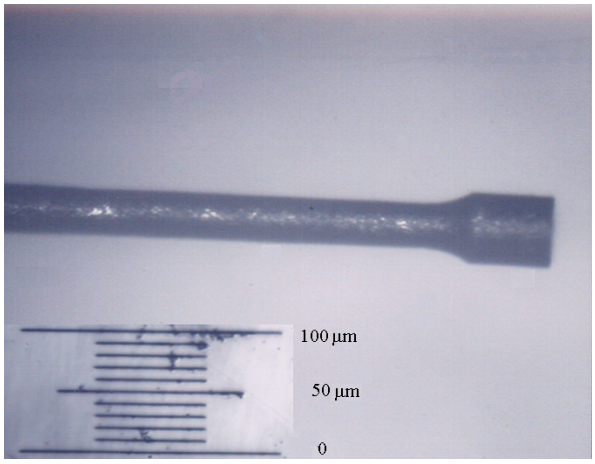

Figure 7 - Probe with cylindrical stylus tip.

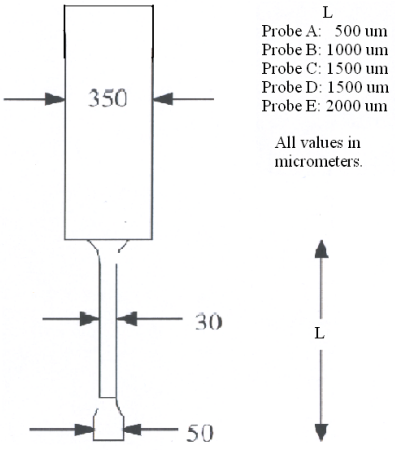

Figure 8 - Example dimensions of cylinder stylus tip probe.

A factor that needs to be accounted for when designing the shaft is the deflection of the upper and lower shafts when a load is applied as shown in Figure 9.

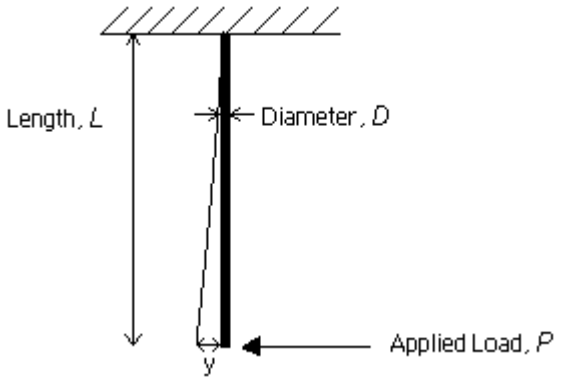

Figure 9 - Beam deflection.

Beam bending theory gives an equation for a beam deflection given by

$$y = \frac{PL^3}{3EI} \tag{4}$$

and the cross sectional bending moment of inertia for a cylinder is given by

$$I = \frac{\pi D^4}{64}, \tag{5}$$

where E is the Young's modulus and all other symbols are defined in Figure 9.

Table 4 below lists the deflections of all the upper and lower shafts using equations (4) and (5) for a force of 1 μN.

Material	Diameter, D (μm)	Length, L (μm)	Deflection, y (nm)
Steel	350	3000	0.06
Steel	30	500	5.42
Steel	30	1000	43.42
Steel	30	1500	146.50
Steel	30	2000	347.30
Tungsten	350	3000	0.03
Tungsten	30	500	2.62

Table 4 - Displacement of a cylindrical beam.

The total deflection, y_T, of the shafts used in these experiments (see Table 7) is given by the deflection of the upper shaft, y_{ur}, plus the deflection of the lower shaft, y_{lr}, or

$$y_T = y_{ur} + y_{lr} . \tag{6}$$

A graph of force against displacement for the lower shaft can be seen below in Figure 10. Since the lower shaft deflects much more than the upper shaft, it can be taken as the total deflection at these dimensions.

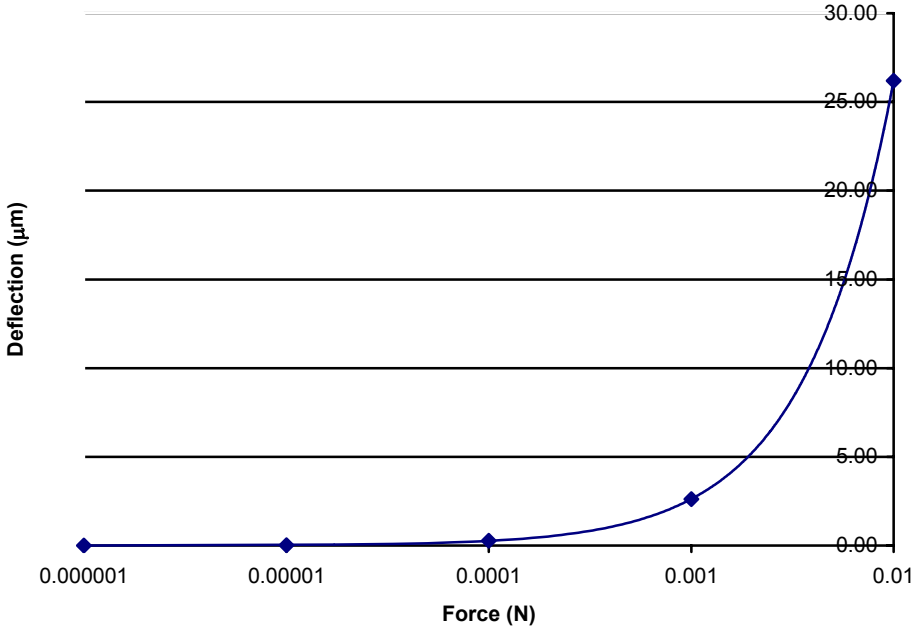

Figure 10 - Graph of deflection against force for the tungsten probe.

The probe should only be allowed to deflect elastically within an acceptable limit to assure the integrity of the probing results. As the diameter decreases and/or the length of the shaft increases, the deflection increases. If the internal stress of the probe exceeds the yield stress of the material the deformation will be plastic and the probe will not return to its original shape after the applied load is removed. The maximum stress in a beam is

$$\sigma_{MAX} = \frac{4PL}{\pi R^3}. \tag{8}$$

So,

$$\sigma_{MAX} \leq \sigma_{YS} \tag{9}$$

and

$$P_{MAX} = \frac{\sigma_{YS}\pi R^3}{4L} \tag{10}$$

where σ_{MAX} is the maximum stress in the shaft, R is the radius of the shaft, σ_{YS} is the yield stress of the shaft material and P_{MAX} is the maximum allowable applied force for elastic deformation. The maximum allowable applied load for elastic deformations can be seen below in Table 5.

Material	Diameter, D (µm)	Length, L (µm)	Yield Stress (MPa)	Maximum Load, P_{MAX} (mN)
Steel	350	3000	500	701.54
Steel	30	500	500	2.65
Steel	30	1000	500	1.33
Steel	30	1500	500	0.88
Steel	30	2000	500	0.66
Tungsten	350	3000	450	631.39
Tungsten	30	500	450	2.39

Table 5 - Allowable applied force for elastic deflection.

4.4 FINITE ELEMENT ANALYSIS

4.4.1 Setting up the simulation

Three different flexure structure types were investigated using finite element analysis: a bent leg flexure structure (see Figure 11), a straight leg flexure structure (see Figure 12) and a solid membrane (see Figure 13). Finite element analysis of the solid membrane and straight leg structures confirmed that they were far too stiff to be practical. It was important for the flexure structure to have a lower stiffness than that for the bending of the shaft in all directions.

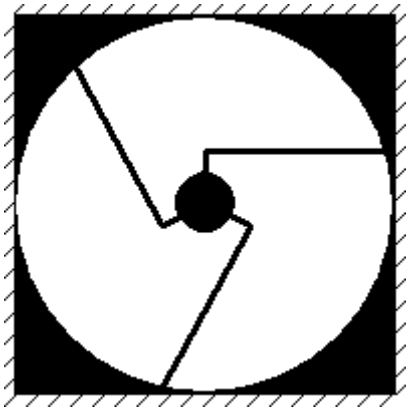

Figure 11 - Bent leg flexure structure.

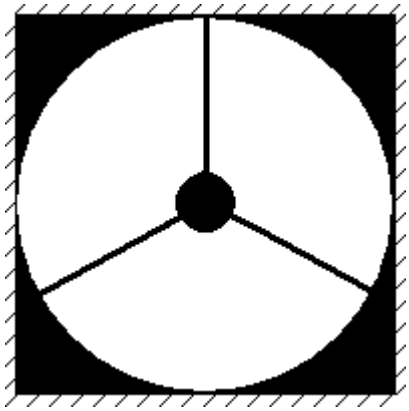

Figure 12 - Straight leg flexure structure.

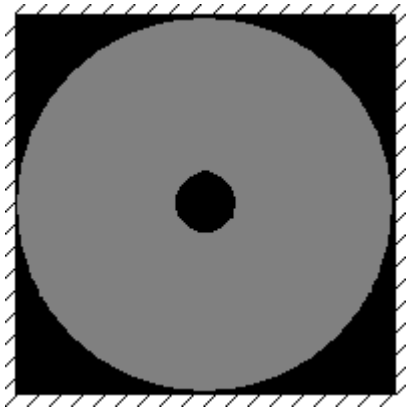

Figure 13 - Solid membrane flexure structure.

Ten different designs of bent leg flexure structure with differing dimensions were modelled using finite element analysis (see Figure 14 and Table 6). During the modelling process, the outside diameter of the flexure structure, a, the diameter of the central island, b, and the length of the legs, c and d, were varied.

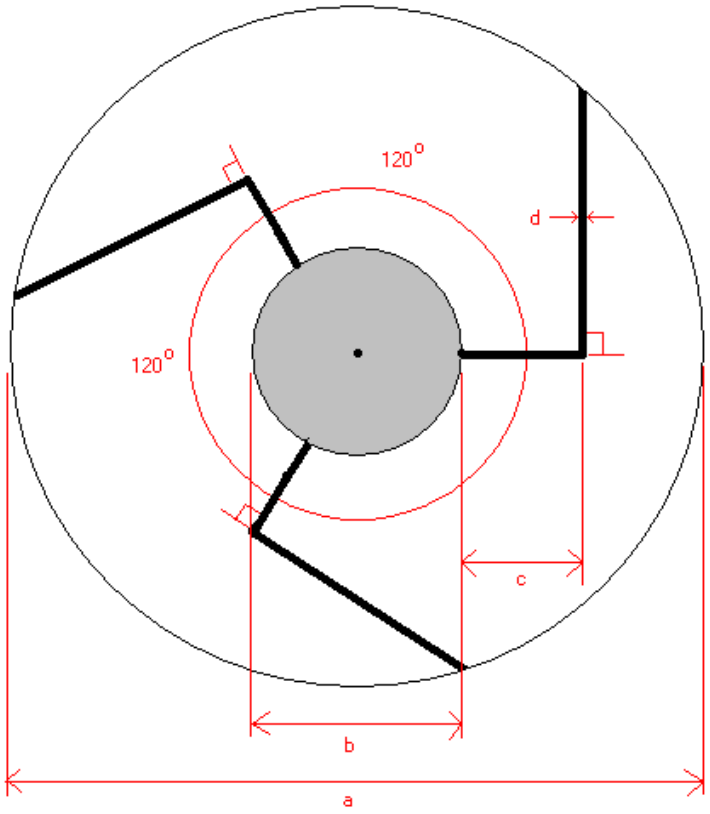

Figure 14 - Dimensions for each case.

Case:	*a* (mm)	*b* (mm)	*c* (mm)	*d* (mm)
1	8	1.5	0.1	0.05
2	8	1.5	0.1	0.1
3	6	1	0.1	0.05
4	6	1	0.1	0.1
5	5	1	0.1	0.05
6	5	1	0.1	0.1
7	4	1	0.1	0.05
8	4	1	0.1	0.1
9	3	1	0.1	0.05
10	3	1	0.1	0.1

Table 6 - Dimensions for variables in Figure 14.

The finite element models are a mixture of triangular and rectangular three-dimensional elements (see Figure 15). Although there were slight variations in the parameters of the finite element model for each different probing system, the central island was modelled using fifteen-node triangular prism elements, the legs were modelled using twenty-node isoparametric brick elements and the legs were joined to the central island with fifteen-node triangular prism elements.

The probe shaft was modelled with three-node conventional beam elements. The upper shaft was modelled as a cylinder with diameter 350 μm and the lower shaft as a cylinder with a diameter of 30 μm. Rigid links were used to reinforce the joint between the central island and the probe to keep the probe normal to the central island at their connection (see Figure 16). The spherical stylus tip was modelled as a mass element with the appropriate mass for a tungsten sphere with a diameter of 50 μm.

The finite element model was used to simulate probing a flat surface in different directions. The simulated probing force caused a specified deflection to the stylus tip in the given direction, positive x, y or z (see the small box in the lower left hand corner of Figure 16 for the orientation of the axes).

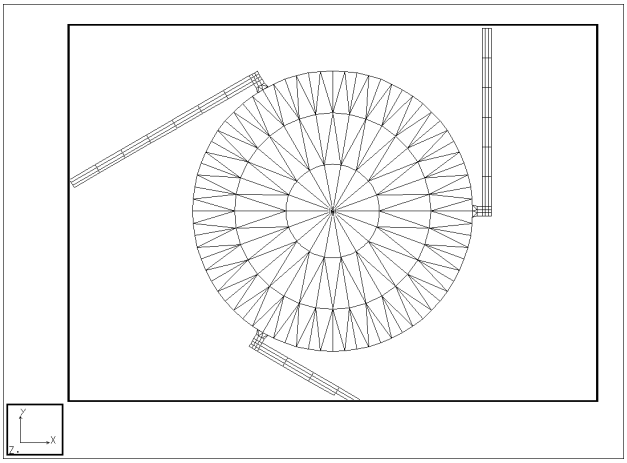

Figure 15 - Finite element screenshot of overhead view of finite element model.

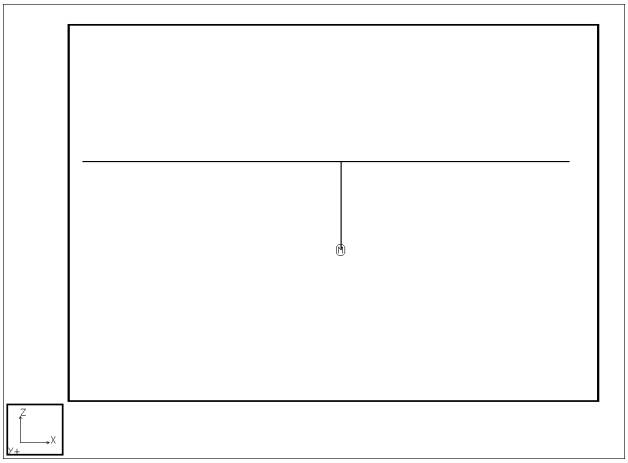

Figure 16 - Finite element screenshot of side view of finite element model.

For an applied force in the *z* direction, the central island should have a vertical deflection in the *z* direction (see Figure 17). For a displacement in the *x* direction, the central island rotates about the *y* axis (see Figure 18) and for a displacement in the *y* direction the central island rotates about the *x* axis (see Figure 19). For a displacement with a (1, 1, 0) vector (an equal displacement in the *x* and *y* directions simultaneously) the central island should be at an equal angle to the *x* and *y* axes (see Figure 20).

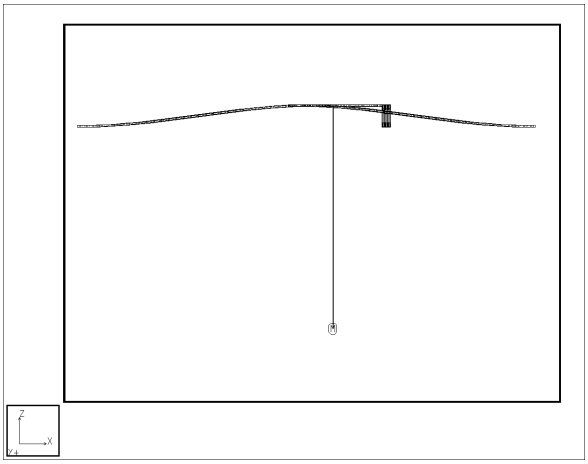

Figure 17 - Displacement in *z* direction.

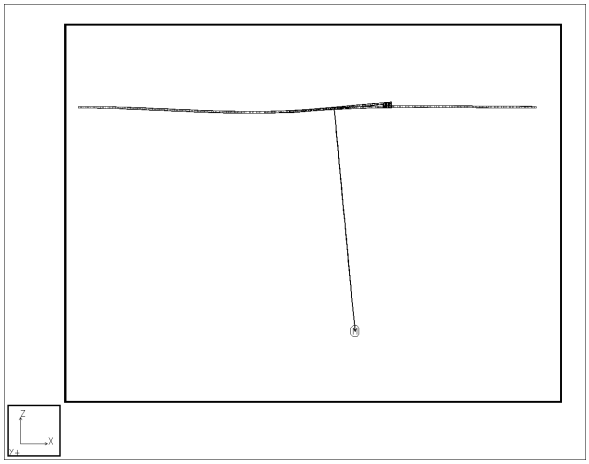

Figure 18 - Displacement in *x* direction.

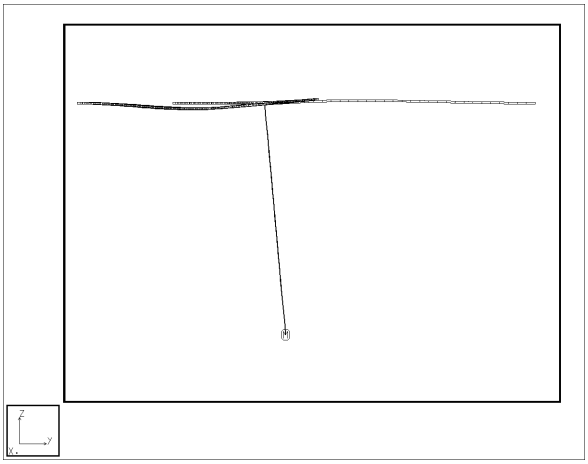

Figure 19 - Displacement in *y* direction.

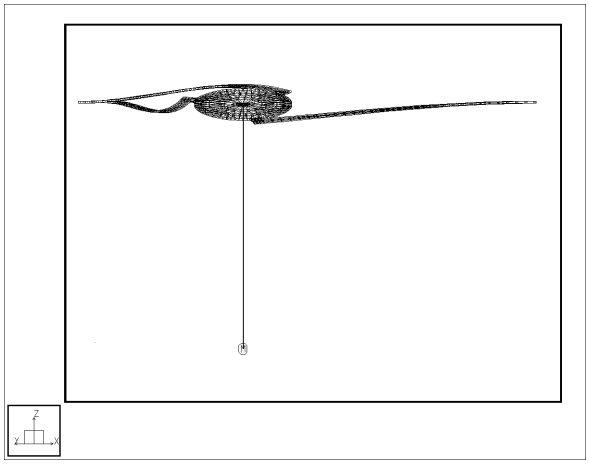

Figure 20 - Displacement in *xy* direction.

4.4.2 Calculation of the stiffness of the probing system

Two components contribute to the stiffness of the probing system: the probe structure and the flexure structure. The stiffness of a cylindrical rod of radius, *R*, in the *x* and *y* directions is given by

$$K_{xy} = \frac{3EI}{L^3}, \tag{11}$$

where the bending moment of inertia for a cylindrical rod is

$$I = \frac{1}{4}\pi R^4. \tag{12}$$

The stiffness of a cylindrical rod in the *z* direction is given by

$$K_z = \frac{AE}{L}, \tag{13}$$

where A is the cross sectional area of the rod. The stiffnesses of the shafts that were used in these experiments are given in Table 7.

Section	L (mm)	D (µm)	K_{xy} (N m^{-1})	K_z (N m^{-1})
Upper shaft	3	350	32 738	12 828 170
Lower shaft	0.5	30	382	565 487
Upper shaft 1	1.941	350	12 0814	19 823 689
Lower shaft 1	1.499	30	14	188 593
Upper shaft 2	1.934	350	122 280	19 903 574
Lower shaft 2	1.014	30	46	278 944
Upper shaft 3	1.879	350	133 199	20 479 165
Lower shaft 3	1.479	30	15	191 130
Upper shaft 4	2.277	350	74 870	16 901 067
Lower shaft 4	0.064	30	183 339	44 28 592
Upper shaft 5	2.662	350	46 833	14 454 283
Lower shaft 5	0.519	30	341	544 704

Table 7 - Probe stiffnesses.

The stiffness of the flexure structures, K, is calculated as

$$K = \omega^2 m \tag{15}$$

where

$$\omega = 2\pi f \tag{16}$$

and f is the resonant frequency of the flexure structure and m is its mass.

A finite element frequency analysis was used to determine the fundamental frequencies of the probing system. From the stiffness values in Table 7 and Table 8 it is apparent that the shafts are stiffer than the flexure structures in all directions.

Table 9 shows the contact force generated when the stylus tip is deflected by 2 µm in the x direction.

Case	Frequency, *f* (Hz)	Mass, *m* (mg)	Direction	*K* (N m^{-1})
1	54.5	4.11	*z*	0.482
	180.0	1.06	*x*	1.355
	180.2	1.06	*y*	1.359
2	76.2	4.20	*z*	0.962
	255.5	1.06	*x*	2.732
	256.2	1.06	*y*	2.747
3	85.6	3.92	*z*	1.133
	208.0	1.04	*x*	1.776
	208.5	1.04	*y*	1.785
4	119.7	3.98	*z*	2.250
	296.0	1.04	*x*	3.597
	297.3	1.04	*y*	3.630
5	112.8	3.91	*z*	1.962
	228.4	1.07	*x*	2.204
	229.1	1.07	*y*	2.217
6	157.8	3.96	*z*	3.892
	324.8	1.07	*x*	4.457
	326.6	1.07	*y*	4.506
7	157.8	3.90	*z*	3.832
	256.3	1.13	*x*	2.930
	257.3	1.13	*y*	2.953
8	221.2	3.94	*z*	7.611
	364.1	1.14	*x*	5.966
	366.6	1.14	*y*	6.048
9	244.4	3.88	*z*	9.146
	299.2	1.26	*x*	4.453
	300.7	1.26	*y*	4.498
10	341.8	3.91	*z*	18.030
	423.1	1.29	*x*	9.116
	426.9	1.29	*y*	9.283

Table 8 - Flexure structure stiffnesses.

Case	Force (μN)
1	2.0
2	4.1
3	2.8
4	5.1
5	3.5
6	6.5
7	4.5
8	8.1
9	5.7
10	11.1

Table 9 - Maximum contact force for a 2 μm stylus tip displacement.

4.5 ASSEMBLY

Several types of materials including silicon, polyimide and metals were investigated for the flexure structures. Due to the use of an optical detection system (see section 4.6), it was necessary for the flexure structure to have a smooth, highly reflective surface. The final designs were manufactured in nickel on silicon.

The flexure structures were manufactured at the Institut für Mikrotechnik, Mainz GmbH (IMM) in Germany. The flexure structures were made using a photo-resist etching process on silicon wafers. Windows were manufactured at the backside of the silicon wafers to define the etch area. Silicon nitride was used as the mask material. Ultra-violet lithography of 20 μm thick resist was used on the front side of the silicon wafer to create a template for the electroplating. Stress optimised nickel electroplating was then carried out to fill out the cavities created by the lithography. The resist was then removed and etching from the back side of the silicon wafer released the flexure structures.

The cylindrical tipped probes from the University of Tokyo were attached at IMM using high precision microrobotics to adhere the probes to the central islands. The spherically tipped probes from the National Taipei University of Technology were attached to the flexure structures at NPL. The probes were held with a pair of tweezers and they were cut down to the required length. The probes were then attached to the flexure structures with epoxy resin. This procedure was carried out with the use of a stereomicroscope and a perspex alignment jig. Perspex was used because it was transparent and allowed the surface of the flexure structure to be seen during alignment of the probes to the centre of the flexure structures.

4.6 OPTICAL DETECTION SYSTEM

An optical detection system was used to detect movements of the probing system (see Figure 21 and Figure 22). The detection system consisted of two independent systems; one that detected the vertical displacement of the central island and one that detected tilting of the

central island. The vertical detection system consisted of a laser diode at a 45° angle to the central island that was focused to a spot on the centre of the island. This spot was then imaged by a microscope objective onto a quadrant photodetector. As the central island was displaced vertically due to an applied force in the *z* direction, the final spot image shifted across the quadrant photodetector causing a change in the output current of the photodetector.

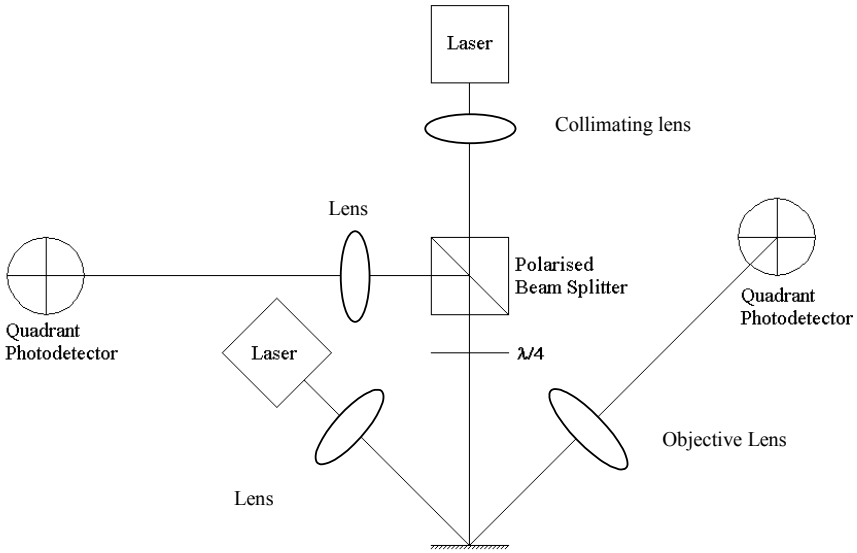

Figure 21 - Layout of the optical detection system.

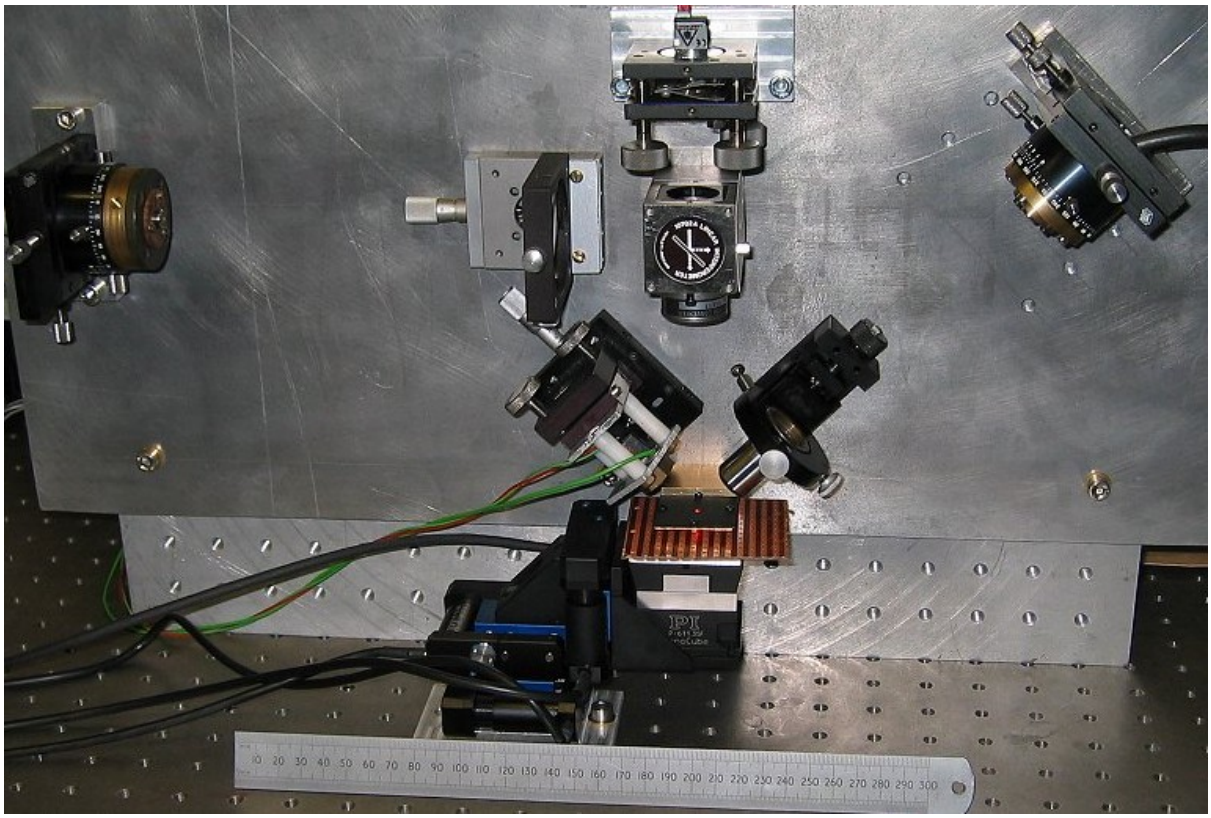

Figure 22 - Photograph of the optical layout.

For the tilt detection system, a collimated beam from a laser diode was passed through a polarising beam splitter, a quarter wave plate, and was incident perpendicularly onto the surface of the central island. The collimated beam was then reflected back through the quarter wave plate and was incident on the polarising beam splitter where it was then reflected at an angle of 90º to its original path. Finally, the beam passed through a lens that focused it onto a quadrant photodetector. The linear polarisation vector of the beam from the laser diode is oriented so that the light from the laser diode is transmitted through the beam splitter. After the beam splitter, the beam passes through the quarter wave plate and is converted in to circular polarisation. The beam is then reflected back through the quarter wave plate. This time when it reaches the beam splitter, the polarisation is linear but orthogonal to the original polarisation and is reflected rather than transmitted by the beam splitter.

4.7 ELECTRONIC DETECTION CIRCUITS

The output from the quadrant photodetectors were electronically processed to provide voltage signals that were proportional to the position of the laser spot on the photodetector. Appendix 1 gives details of the electronic circuits.

4.8 SOFTWARE CONTROL AND TRANSLATION STAGE

The output voltages from the electronic detection circuits were sent to a National Instruments Field Point analogue-to-digital converter module. A computer program was written in Microsoft Visual Basic version 6.0 to read the output voltages from the Field Point Explorer module, write the data to a user-defined output file and plot the data on the computer screen. The program also used commands to interact with the Physik Instrumente M-110 micro translation stages. These stages were set up as a three orthogonal axes stage system (see Figure 23) allowing motion in the *x*, *y* and *z* directions with a smallest incremental step size of 50 nm and a total travel range of 5 mm. See Figure A3 in Appendix 1 for further specifications of the stage.

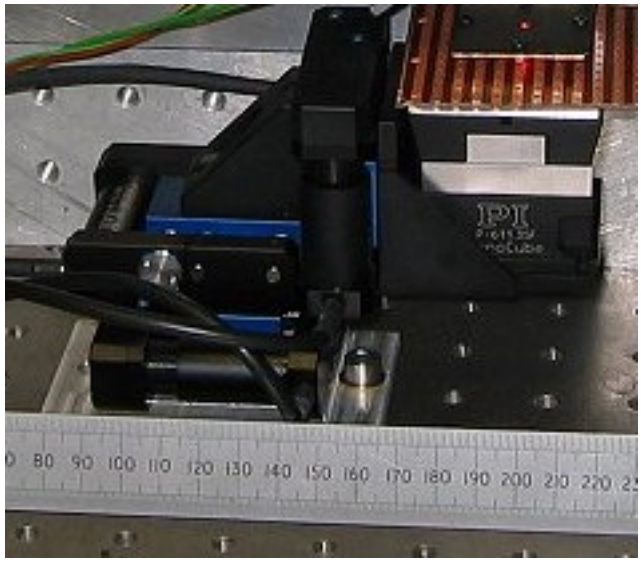

Figure 23 - Physik Instrument three axes micro translation stages.

5 EXPERIMENTAL RESULTS

5.1 REPEATABILITY TESTS

To test the repeatability of the probing system, the stylus tip was used as a touch-trigger probe (see section 2.2), *i.e.* the probe is used merely to indicate when the stylus tip has contacted the surface. The stylus tip was brought into and out of contact with a polished and lapped test surface numerous times and the point of contact (on) and the subsequent point of non-contact (off) were recorded for the *x*, *y* and *z* axes.

To calculate the repeatability the standard deviation of the difference between the on and off measurements was determined. The values of the repeatability were 0.252 μm, 0.239 μm and 0.260 μm and the *x*, *y* and *z* axes respectively.

The Physiks Instrumente documentation lists the uniaxial repeatability for the micro-translation stages as 0.1 μm and the backlash as 2 μm. To reduce the effects of backlash the probing was always carried out from the same direction. Factors that contribute to the repeatability of the probing system include: permanent bends in the probe stem, the surface roughness of the stylus tip and the surface, electronic noise and seismic vibration of the probing system.

5.2 MEASUREMENTS OF SMALL HOLES

The probing system was used to measure *x* and *y* co-ordinates of the edges of a hole. A stylus with a spherical tip, an upper shaft length of 3 mm, and a lower shaft length of 0.5 mm was used. The first hole measured was in a metal hub used for medical applications (see Figure 24). The roundness of the central hole on the smaller (left) end of the hub was measured.

Figure 24 - Metal hub.

Measurements were taken in steps around the perimeter of the hole with the probe deflecting on to the surface approximately 2 µm (see trial 1 in Figure 25).

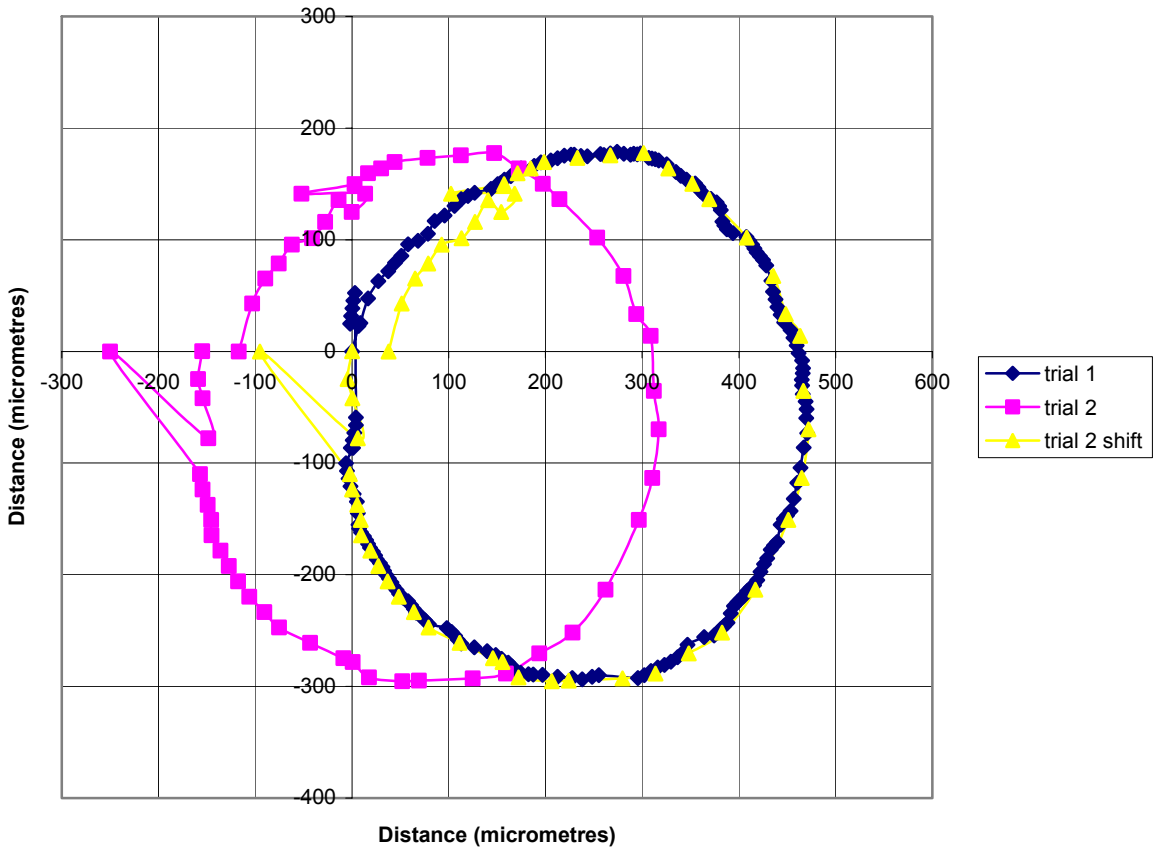

Figure 25 - Results from measurements of a metal hub.

An average diameter (ignoring outliers) was calculated as 475 µm (D_m). However, this average diameter did not take into account the nominal radius of the probe (r = 25 µm) and the deflection of the probe onto the surface ($y \approx 2$ µm). These corrections can be accounted for using the equation for the corrected diameter as

$$D_{corr} = D_m + 2r - 2y\,. \tag{18}$$

Once all corrections had been applied the diameter was calculated to be 521 µm.

A repeat measurement was made of the metal hub (see trial 2 in Figure 25) and the average diameter from the measurements was 469 µm, giving a diameter of 515 µm once all corrections had been applied.

The engineering drawings for the hub specified the diameter of the hole to be 490 µm ± 50 µm. A vertical scanning white light interferometer [40] (Taylor Hobson Talysurf CCI 3000 model) measured an average diameter of 534 µm. The CCI results can only be considered an indication due to the difficulties in judging the diameter from the height plot and setting the cursors to the hole edge on the profile plot. The probing system and the white

light interferometer disagree by an average of 16 µm but are probably measuring at different positions along the bore of the hole.

Trial 2 shift in Figure 25 is the data from trial 2 shifted in the *x* direction to see an overlay of the data from trial 2 with trial 1.

Further measurements were made on a ceramic tube used for terminating a fibre optic cable. The average diameter measured with the probe for trial 1 was 79 µm, giving a diameter of 125 µm once all corrections had been applied (see trial 1 Figure 26).

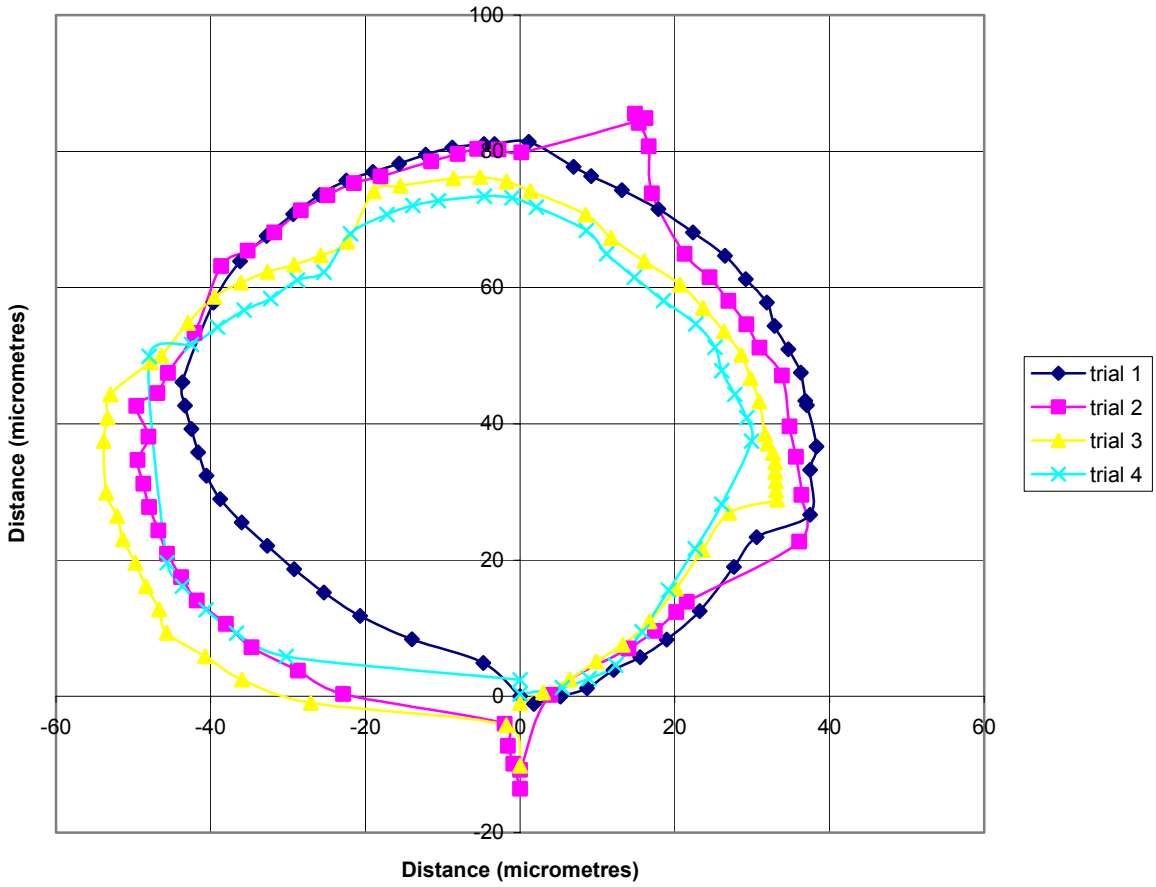

Figure 26 - Results from measurements of a ceramic tube.

Further measurement were made of the ceramic tube, see trials 2 to 4 in Figure 26. The average diameter of the four trials, after applying the appropriate corrections was 128 µm. The vertical scanning white light interferometer measured the diameter as 127 µm.

6 FUTURE RECOMMENDATIONS

In general, the probe that was developed and tested as part of this project has proved that the three-legged flexure structure is a sound design. However, there are several component parts of the design that could be improved upon. Further characterisation work should be carried out to determine the accuracy and precision of the measurements with the probe in all axes.

The optical detection system will need to be optimised and made much more compact. It may even be possible to include capacitive sensors into the leg design as discussed in section 3.2. The noise level of the electronics will be improved by using more stable components and further filtering. The ability to collect data from the probe and analyse the results also needs to be improved upon with better interfacing protocols and more user-friendly software. In the future, the aspects of the rest of the micro-CMM need to be considered in detail.

7 ACKNOWLEDGMENTS

The authors would like to thank Keith Jackson, Jane Haycocks, Dr Andrew Lewis, and Nigel Cross at NPL for help with the project and for useful discussions. The authors would also like to thank David Flack for making the final corrections. The work was funded under NPL Strategic Research project 9SRP4080.

8 REFERENCES

1. Taniguchi N 1996 *Nanotechnology; Integrated Processing Systems for Ultra-precision and Ultra-fine Products* (Oxford University Press, Oxford, UK)

2. Rai-Choudhury P 2001 *MEMS and MOEMS Technology and Applications* (SPIE The International Society for Optical Engineering, Bellingham, USA)

3. Ruijl T, Franse J, van Eijk J 2001 Ultra precision CMM aiming for the ultimate concept *Proc. 2nd euspen Int. Conf., Turin, Italy* 234-237

4. Jäger G, Manske E, Hausotte T 2001 Nanopositioning and measuring machine *Proc. 2nd euspen Int. Conf., Turin, Italy* 290-293

5. Peggs G N, Lewis A J, Oldfield S 1999 Design for a compact high-accuracy CMM *Ann. CIRP* **48** 417-420

6. Bergmans R H 2002 Metrology for nanotechnology *Proc. 3rd euspen Int. Conf., Eindhoven, The Netherlands* 557-560

7. Leach R K, Haycocks J, Jackson K, Lewis A J, Oldfield S, Yacoot, A 2001 Advances in traceable nanometrology at the National Physical Laboratory *Nanotechnology* **12** R1-R6

8. Gardner J W, Varadan V K, Awadelkarim O O 2001 *Microsensors, MEMS and Smart Devices* (Wiley & Sons Ltd., Chichester, U.K)

9. Bryan J B 1979 The Abbé Principle revisited *Prec. Eng*. **1** 129-132

10. Vermeulen M M P A, Rosielle P C J N, Schellekens P H J 1998 Design of a high-precision 3D-coordinate measuring machine *Ann. CIRP* **47** 447-451

11. Weekers W G, Schellekens P H J 1995 Assessment of dynamic errors of CMMs for fast probing *Ann. CIRP* **44** 469-474

12. van Vliet W P, Schellekens P H J 1996 Accuracy limitations of fast mechanical probing *Ann. CIRP* **45** 483-487

13. Pril W O, Struik K G, Schellekens P H J 1997 Development of a 2D probing system with nanometer resolution *Proc. 16th ASPE* 438-442

14. Haitjema H, Pril W O, Schellekens P H J 1997 Development of a silicon-based nanoprobe system for 3-D measurement *Ann. CIRP* **50** 365-368

15. Kleine-Besten T, Loheide S, Brand U, Bütifisch S, Büttgenbach S 1999 Development and characterisation of new probes for dimensional metrology on microsystem components *Proc. 1st euspen Int. Conf.*, *Bremen, Germany* 387-390

16. Pornnoppadol P, Cao S, Schmidt M, Wilke R, Bütifisch S, Nesterov V, Brand U 2002 Three-dimensional microprobe with reduced probing forces *Proc. 3rd euspen Int. Conf., Eindhoven, The Netherlands* 737-740

17. Enami K, Hiraki M, Takamasu K 2000 Nano-probe using optical sensing *IMEKO World Congress, 16th International Measurement Confederation* **8** 79-82

18. Furutani R, Young-Won C 2001 High resolution probe system for CMM *Proc. 2nd euspen Int. Conf., Turin, Italy* 246-249

19. Schwenke H, Waldele F, Weiskirch C, Kunzmann H 2001 Opto-tactile sensor for 2D and 3D measurement of small structures on coordinate measuring machines *Ann. CIRP* **50** 361-364

20. Matsuoka H, Kasei S, Hinohara M 2002 Development of a resonance-based touch probe structured with 2 parallel cross-shaped thin leaf springs *J. Japanese Soc. Prec. Eng.* **68** 269-273

21. Kim B, Masuzawa T, Bourouina T 1999 The vibroscanning method for the measurement of micro-hole profiles *Meas. Sci. Technol.* **10** 697-705

22. Vidic M, Harb S M, Smith S T 1998 Observation of contact measurements using a resonance-based touch sensor *Prec. Eng.* **22** 19-36

23. Takamasu K, Kuo C-C, Suzuki A, Hiraki M, Furutani R, Ozono S 1999) Development of a pneumatic ball probe *Int. J. Japan Soc. Prec. Eng.* **33** 233-238

24. Takaya Y, Shimizu H, Takahashi S, Miyoshi T 1999 Fundamental study on the new probe technique for the nano-CMM based on the laser trapping and Mirau interferometer *Measurement* **25** 9-18

25. Ashkin A, Dziedzic J M 1971 Optical levitation by radiation pressure *Appl. Phys. Lett.* **1941** 283-290

26. Dong W P, Mainsah E, Sullivan P J, Stout K J 1994 *Three-dimensional surface topography: Measurement, interpretation and applications (*Penton Press, London)

27. Buning J H, Herriott D R, Gallagher J E, Rosenfeld D P, White A D, Brangaccio D J 1974 Digital wavefront interferometer for testing optical surfaces and lenses *Appl. Opt.* **23** 2693-2703

28. Zygo Corporation 2002 *Newview 5000 Customer Data Sheet* (Zygo Corporation, Middlefield, Connecticut, USA)

29. Whitehouse D J 1999 *Laser Metrology and Machine Performance IV* (WIT Press, Southampton, UK) 267-276

30. Binnig G, Röhrer H 2000 Scanning tunneling microscopy *IBM J. Research Develop.* **44** 279-293

31. Binnig G, Quate C F, Gerber C 1986 Atomic force microscope *Phys. Rev. Lett*. **56** 930-933

32. Meyer G, Amer N M 1988 Novel optical approach to atomic force microscopy *Appl. Phys. Lett*. **53** 1045-1047

33. Haycocks J A, Jackson K 2001 A metrological atomic force microscope for calibration of transfer standards *Proc. 2nd Int. Conf. euspen, Turin, Italy, 27th – 31st May* 392-395

34. Pohl D W 1990 Scanning near-field optical microscopy *Advances in Optical and Electron Microscopy 12* (Academic Press, London)

35. VanLandingham M 1998 The effect of instrumental uncertainties on AFM indentation measurements, University of Delaware, *Discussion of uncertainties published on the Web,* (www.mobot.org/jwcross/spm/)

36. Serry F M, Nagy P J, Horowitz J, Oden P I, Heaton M G 2002 3D MEMS metrology with the atomic force microscope *Veeco Metrology Group Information Leaflet* (Veeco Instruments Inc.)

37. Puttock M J, Thwaite E G 1969 *Elastic Compression of Spheres and Cylinders at Point and Line Contact* National Standards Laboratory Technical Paper No. 25, (Division of Applied Physics, CSIRO, New South Wales, Australia)

38. Material Properties Database: http://www.matweb.com

39. Masuzawa T 2000 State of the art in micromachining *Ann. CIRP* **49** 473-488

40. Leach R K, Lee-Bennett I 2004 Characterisation of a new vertical scanning white light interferometer – a test case? *XIth Int. Colloq. Surfaces, 2 – 3 Feb., Chemnitz, Germany* 11-18

APPENDIX 1 – CIRCUIT DIAGRAMS AND PI STAGE SPECIFICATIONS

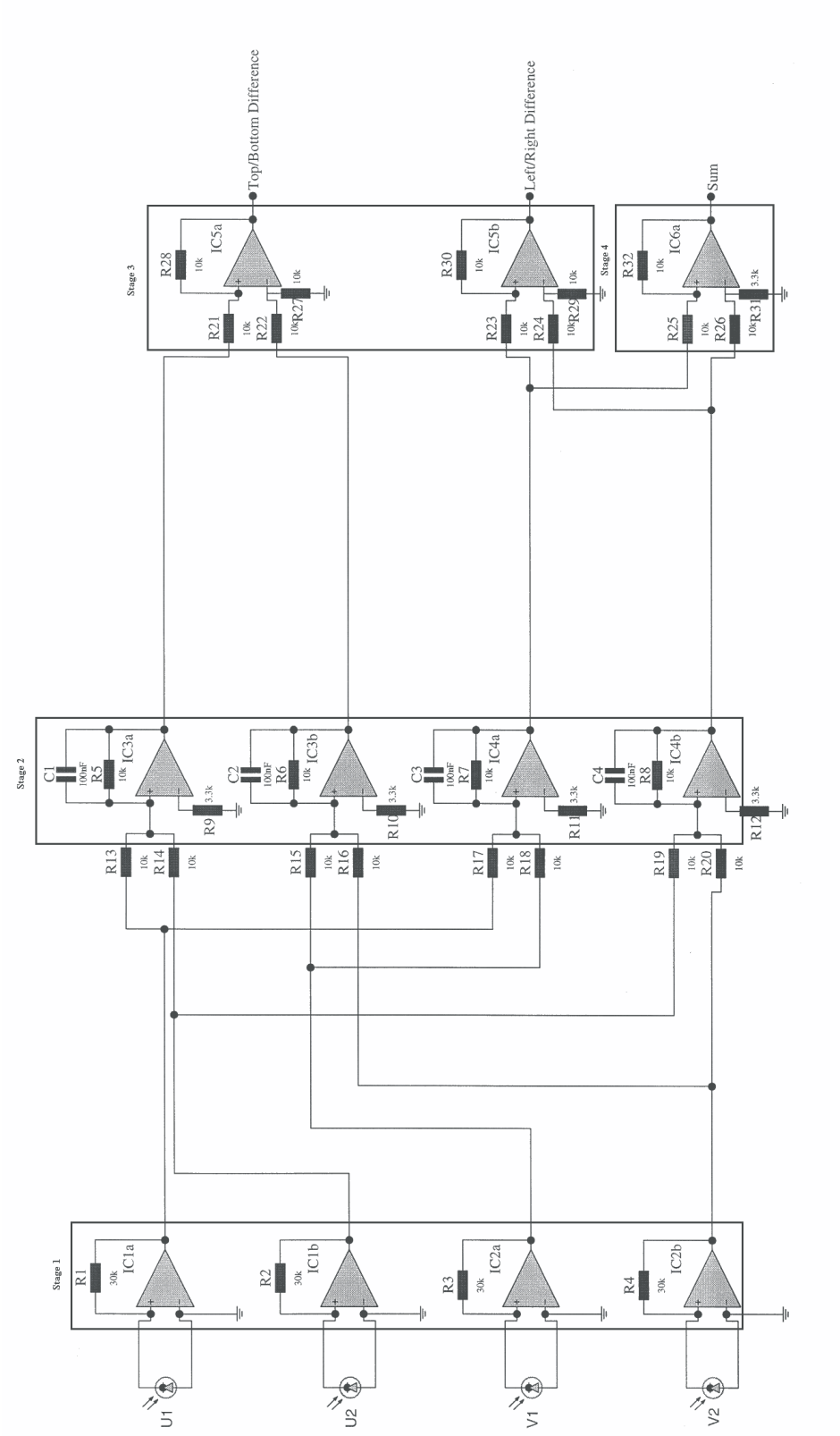

Figure A1 – Vertical detection circuit diagram.

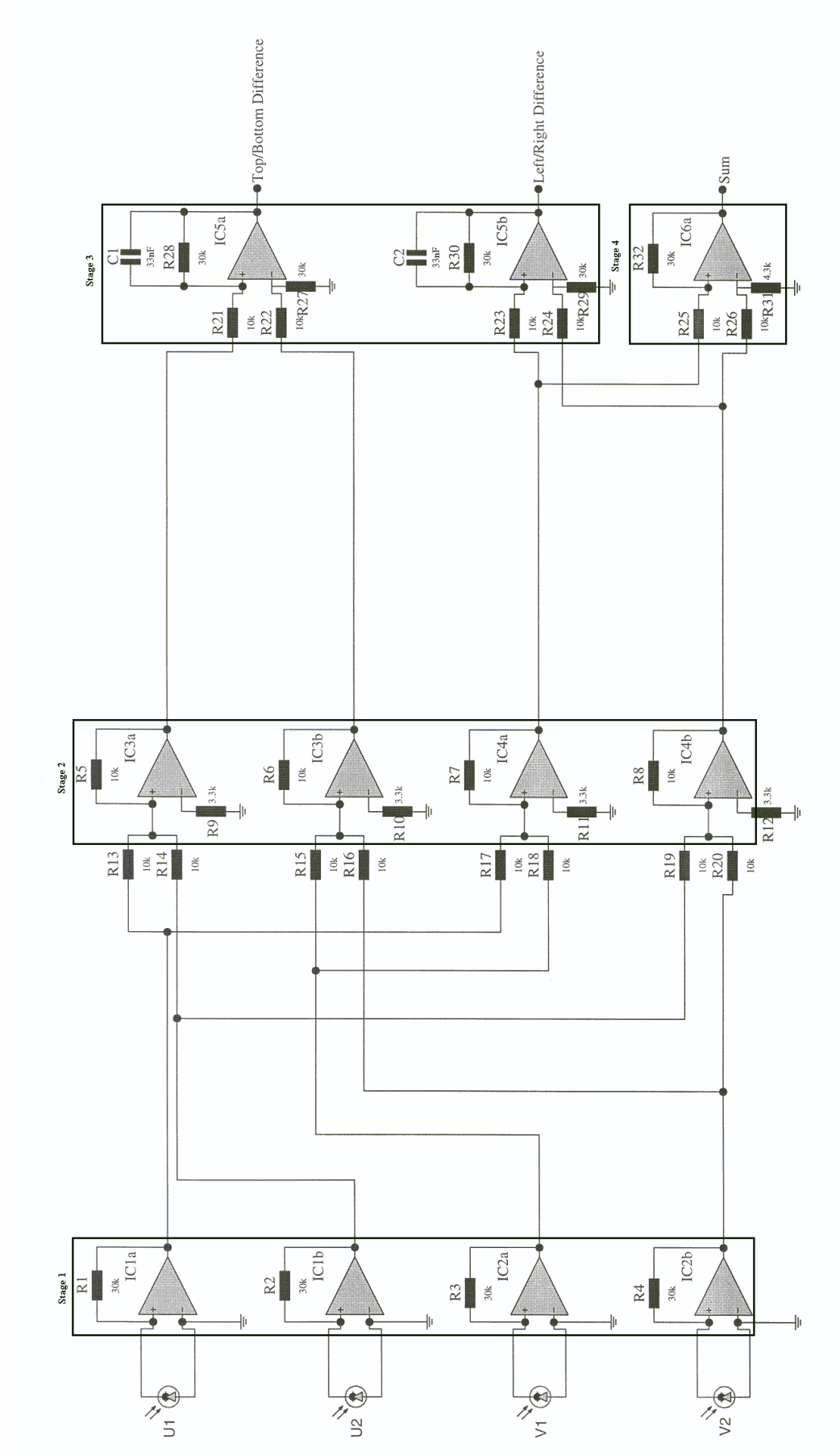

Figure A2 – Tilt detection circuit diagram.

2 M-110 M-111 Technical Data

Technical Data

Models	M-110.1DG	M-111.1DG	M-110.12S	M-111. 12S	Units
Travel range	5	15	5	15	mm
Design resolution	0.007	0.007	0.006	0.006	µm
Min. incremental motion	0.05	0.05	0.05	0.05	µm
Unidirectional repeatability	0.1	0.1	0.1	0.1	µm
Backlash	2	2	2	2	µm
Max. velocity	1.5	2.5	1	1	mm/sec
Max. normal load capacity	10	10	10	10	kg
Max. push/pull force	10	10	10	10	N
Max. lateral force	10	10	10	10	N
Encoder resolution	2048	2048	-	-	counts/rev.
Motor resolution	-	-	2400*	2400*	steps/rev
Drive screw pitch	0.4	0.4	0.4	0.4	mm/rev.
Gear ratio	28.44444:1	28.44444:1	28.44444:1	28.44444:1	
Nominal motor power	0.6	2	*	*	W
Motor voltage range	0 to ±12	0 to ±12	24*	24*	V
Weight	0.3	0.4	0.3	0.4	kg
Recommended motor controllers	C-842, C-844, C-860	C-842, C-844, C-860	C-600, C-630	C-600, C-630	

**2-phase stepper, 24 V chopper voltage, 2,400 microsteps with C-600, C-630 controllers*

	M-110.1DG	M-111.1DG	
Nominal travel range:	729,090	2,187,271	[counts]

Precise Numbers :

Gear head ratio: (28 + 4/9) :1

Translation Ratio: 145.63555 counts / µm

Design Resolution: 0,006866455 µm / count

Figure A3 – PI micro translation stage specifications.